HOKKAIDO UNIVERSITY

Title	Gas-like Bosonic states formed around 160 core nucleus close to the 2α decay threshold energy
Author(s)	YA MIN HTET
Degree Grantor	北海道大学
Degree Name	博士(理学)
Dissertation Number	甲第16748号
Issue Date	2026-03-25
DOI	https://doi.org/10.14943/doctoral.k16748
Doc URL	https://hdl.handle.net/2115/99593
Type	doctoral thesis
File Information	YA_MIN_HTET.pdf, 全文

Hokkaido University Collection of Scholarly and Academic Papers : HUSCAP

Doctoral Dissertation

Gas-like Bosonic states formed around ^{16}O core nucleus close to the 2α decay threshold energy

(2α崩壊しきい値近傍の^{16}Oコア核のまわりに形成されるガス的ボソン状態の研究)

YA MIN HTET

Graduate School of Science, Hokkaido University
Department of Cosmoscience

2026 March

Acknowledgement

I am deeply grateful to my supervisor, Prof. M. Kimura, for his valuable supports, guidance, encouragement, and insightful advice throughout my research.
I would like to also express my sincere thanks to Prof. K. Nomura for his essential guidance and support.
I would like to thank to my former supervisor, Prof. W. Horiuchi, whose helps greatly to improve the initial development of this work and my understanding of the physic involved.
I would like to express my sincere thanks to Dr. Bo Zhou, Dr. Qing Zhao and
Dr. T. Oishi for their contributions and encouragement.
I owe my deepest gratitude to Dr. H. Moriya and M. Homma for their support.
I could not have completed this work without the unwavering support of my supervisors and colleagues.
I am profoundly thankful to my parents, who gave me the constant encouragement sustained me throughout this entire process.
Lastly, I offer my regards and blessings to all of those who supported me in any respect during the completion of this work.

Abstract

Nuclear clustering is the most unique and interesting phenomena observed in various physical aspects. In studies of nuclear clustering phenomena, the Hoyle state, an excited state of ^{12}C located at 7.65 MeV, is a representative example of carbon production in a stellar environment through the triple-alpha process. In recent years, it has been suggested that the Hoyle state exhibits characteristics of a Bose-Einstein Condensate (BEC), attracting considerable interest from both theoretical and experimental perspectives. Two challenging questions arise: what is the maximum number of α clusters for multi-α condensation and how can these multi-cluster systems overcome the inherent instabilities present in heavier nuclei?

In a multi-α condensed system, theoretical studies have reported that the maximum number of α particles is limited to approximately ten. A reasonable solution to this instability problem is assuming the presence of the Core nucleus that provides an additional attractive potential. Exploring the possibility of α condensation around a core nucleus represents a new and intriguing class of nuclear clustering. Previous theoretical investigations, T. Ichikawa et al. have predicted plausible ^{16}O+2α condensed states based on an interesting idea. However, the strong mixing with physically unimportant configurations (non-resonant states) in their result made the identification of true resonant states non-trivial.

To address this issue, we aim to provide a more robust theoretical verification of the ^{16}O+2α condensation. Our objective is to clearly identify the resonant states in which α particles condense around an inert core nucleus by extending the limitation of previous study. Furthermore, we attempt to predict the properties of resonant candidates, such as the resonance energies and α-decay widths.

As numerical methods, the real-time evolution method (REM) and the analytical continuation in the coupling constant (ACCC) method were applied in our calculations. The REM method has a good opportunity for investigating the ground state and excited cluster state of atomic nuclei. We employ the real-time evolution method (REM), which generates physically important basis states using the equation of motion, minimizing contamination from the continuum (physically unimportant configurations). The analytical continuation in the coupling constant (ACCC) method also includes a simple calculation and it was used to estimate the characteristics of the resonance states (the α-decay widths).

Our REM calculations yield significantly improved and stable results than the previous calculation, and identify resonance states clearly. The numerical results show reasonable agreement with previous work by T. Ichikawa et al. and firmly establish candidates for the ^{16}O+2α condensed state. The 0_3^+ and 0_4^+ eigen states were identified as strong candidates of resonance states. The isoscalar monopole transition strength, B(IS0) from the ground state to the 0_3^+ and 0_4^+ states, are remarkably strong supporting their nature as spatially extended ^{16}O+2α condensate state. These findings are consistent with the predictions of T. Ichikawa et al. The root-mean-square radii of these two eigen states are approximately 3.0 fm, also in good agreement with T. Ichikawa et al. These radii seem small compared to the root-mean-square radius of Hoyle state of ^{12}C (3.7 fm). For this reason, the distribution of valence 2α in the 0_3^+ and 0_4^+ eigen states are calculated. It suggests that the α particles trapped between the surface of the core nucleus and the Coulomb barrier. Furthermore, the calculated α-decay widths of these states are small, indicating that experimental observation should be feasible.

Finally, we performed a theoretical investigation of core nucleus plus 2α condensates, representing a novel type of α clustering. By reducing the substantial mixing with the continuum, we achieved the clear identification of real resonance states. Our results show the reasonably agreement with previous work and firmly establish the 0_3^+ and 0_4^+ states, located approximately 5 MeV and 1 MeV below the ^{16}O+2α threshold, as the candidates for 2α condensation around the ^{16}O core nucleus. We have demonstrated that the real-time evolution method (REM) is effective in identifying these gas-like bosonic states of 2α condensation around the core nucleus ^{16}O.

Contents

List of Figures

Chapter 1

Introduction

1.1 Fundamental properties of atomic nucleus

1.1.1 Discovery of Nucleus

In 1904, J. J. Thomson proposed "Plum Pudding Model" as the first atomic structure of elements. The atom is described as a uniform sphere of positively charge (pudding) and the negatively charged electrons are embedded or scattered (plum) within it. The atom is electrically neutral because the total amount of positively charged sphere balances with negatively charged electrons. Since, this model failed to explain certain experimental results associated with the atomic structure of elements. In 1909, Ernest Rutherford directed the Geiger-Marsden experiment by bombarding a thin sheet of gold foil with α-particles and studied the trajectory of these particles after their interaction with the gold foil. Based on the observations, Rutherford proposed the atomic structure of elements as shown in fig 1.1.

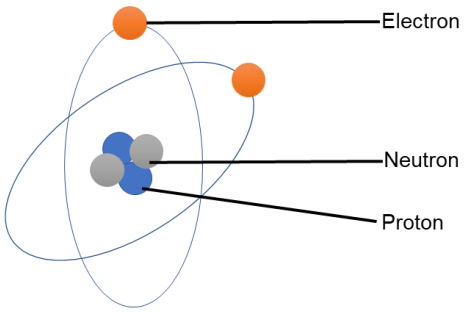

Figure 1.1: Rutherford's atomic model diagram

According to Rutherford's nuclear model, an atom consists of a positively charged nucleus, which is concentrated at the center of the atom and is surrounded by a cloud of negatively charged electrons in defined energy levels or orbitals. The attractive electromagnetic force between negatively charged electrons and the positively charged nucleus keeps electrons bound to the atom, causing them to occupy regions around the nucleus known as orbitals. An electron is a fundamental particle that is not composed of smaller constituents (quarks).

The atomic nucleus is made up of two types of subatomic particles namely nucleons: positively charged protons and electrically neutral neutrons. Unlike electrons, both proton and neutron are composed of three elementary particles called quarks. The internal structure of proton consists of two up quarks and one down quark (uud), while a neutron consists of one up quark and two down quarks (udd). When the number of protons equals the number of electrons, the positive and negative charges cancel each other out, making the atom electrically neutral.

The chemical element of an atom is determined by the number of protons in its nucleus, which is known as the atomic number (Z). The element oxygen has an atomic number Z=8, while carbon has Z=6. The mass number A of the nucleus is the sum of the number of protons and neutrons (A=Z+N), where N is the number of neutrons. The nucleus is represented by

$$^{A}_{Z}X$$

where, X represents the chemical element. For example, the symbol $^{16}_{8}O$ means that oxygen nucleus contains eight protons and eight neutrons.

The discovery of the nucleus showed that atoms are mostly empty space with a small, dense center. The Geiger-Marsden experiment changed earlier ideas about atomic structure and helped scientists better understand the nature of nuclear matter.

1.1.2 Nuclear mass, radius, binding energy, threshold energy

The atomic nucleus is the central core of an atom, containing protons and neutrons and accounting for nearly all of its mass. Understanding nuclear properties such as nuclear mass, nuclear radius, binding energy, and threshold energy is essential for explaining nuclear stability, reactions, and energy production. Nuclear mass provides insight into mass defects, while nuclear radius reveals information about nuclear size and density. Binding energy represents the energy that holds the nucleus together, and threshold energy defines the minimum energy required for certain nuclear reactions to occur. Together, these concepts form the foundation of nuclear physics and are crucial in both theoretical studies and practical applications such as nuclear power and particle accelerators.

(i) Nuclear Mass and binding energy

The nuclear mass $\mathrm{M_{nucl}}$ is obtained from the atomic mass M by subtracting the masses of the Z orbital electrons m_e from the atomic mass.

$$\mathrm{M_{nucl}} = \mathrm{M} - \mathrm{Zm_e}$$

Almost all the mass of atom comes from the nucleus because the electron mass is negligible as compared to proton and neutron. Although the nucleus is small in size compared with the atom, the nucleus is very dense. It has been observed that the mass of a nucleus is less than the total mass of its individual protons and neutrons if they were free and not bound together. This difference is a measure of the nuclear binding energy that holds the nucleons as a nucleus, and is known as the mass defect Δm.

In 1905, Albert Einstein first derived the relation between mass and energy from his special theory of relativity. The binding energy of a nucleus is the total energy required to separate all the nucleons in the nucleus. The nuclear binding energy is calculated by the relationship BE=$\Delta \mathrm{mc}^2$, where c is the speed of light. It shows that mass and energy are interchangeable due to the large value of c^2. Let M_p be the rest mass of a proton, M_n is the rest mass of neutron and M_N is the rest mass of the nucleus; Z is the atomic number and A is the mass number of the nucleus.

$$\mathrm{BE} = [\mathrm{ZM}_p + (A - Z)\mathrm{M_n} - \mathrm{M}_N]\mathrm{c}^2$$

The binding energy of ^{4}He nucleus can be calculated as follows.

$$\mathrm{BE}(^4\mathrm{He}) = [2 \times 1.007276 + 2 \times 1.008665 - 4.002603]\mathrm{c}^2 \times \frac{931.49\mathrm{MeV}}{\mathrm{c}^2}$$

$\mathrm{BE}(^4\mathrm{He}) = 28.2956\mathrm{MeV}$
$\mathrm{BE}(^4\mathrm{He})/A = 7.0739\mathrm{MeV}$

The mean binding energy per nucleon is calculated as BE/A as shown in fig 1.2. [1] Most of the nuclei have an average binding energy per nucleon of 7.5 to 8.9 MeV. The mean binding energy per nucleon of the nucleus at central region (A=40 to 100) is nearly constant at about 8.5 MeV/nucleon. For light elements region (A<20), binding energy per nucleon shows irregular or fluctuating patterns due to nuclear shell effects, paring of nucleons and magic number.

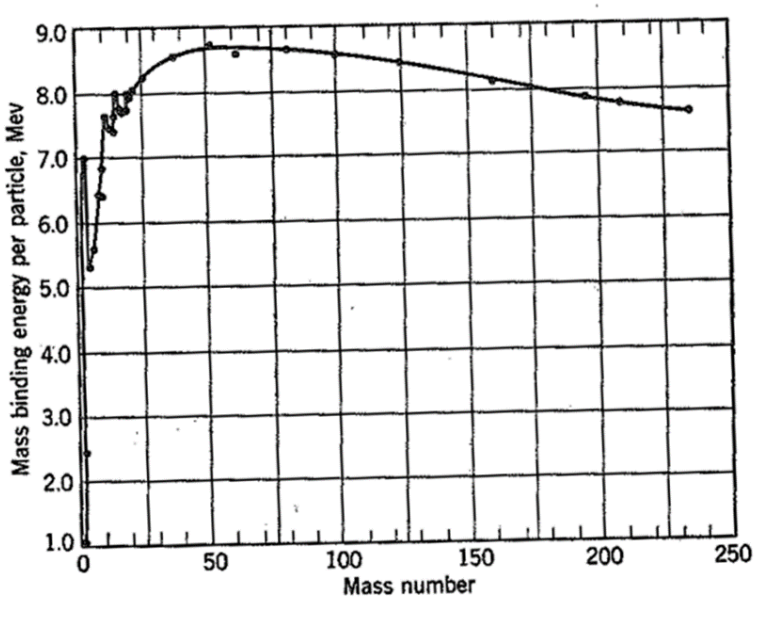

Figure 1.2: The mean binding energy per nucleon for the most stable nucleus at each mass number

The mean binding energy per nucleon is a direct indicator of the stability of a nucleus. The exceptional nuclear binding energy per nucleon is found in low mass number region such as ^{4}He, ^{12}C, ^{16}O, etc. The higher binding energy per nucleon means that each nucleon is more tightly bound within the nucleus making the nucleus more stable. Therefore, the amount of binding energy per nucleon can roughly determine the stability of the desired nucleus.

(ii) Nuclear radius and density

The nuclear radius is a fundamental property that describes the size of an atomic nucleus. A nucleus is often represented as a spherical shape in various theoretical nuclear models. A variety of different shapes in nuclei have been predicted according to the proportion of proton to neutron number ratio, condition of excitation energy and spin of specific nucleus. The magic nuclei which are composed of magic number of proton and neutron (2,8,20,28,..) have a spherical shape since both protons and neutrons fully fill out their quantum state. The nuclear ground state is generally determined as a spherical shape but other excited state may be deformed from spherical shape upon various conditions.

Electron diffraction had been used in finding the radii of various nuclei with different atomic number of element. Electrons are accelerated in an electric field across through several hundred megavolt (400 MV). These high energy electrons passed through a thin sheet of a solid material in vacuum and the detector is used to record the arrivals of electrons at different angles θ on the other sides. The radius of nucleus is calculated by using the detected angles θ and de Broglie wavelength λ such as the relation r $\sin\theta$=0.61λ. After precise investigations of nuclear radii have been carried out for a wide range of nuclides, the nuclear radius is generally given by the following formula

$$R = 1.2 \times A^{1/3}\text{fm}$$

The volume of a nucleus is proportional to the number of nucleons it contains. Using the nuclear radius, the volume of a nucleus, V, can be expressed as

$$V = \frac{4}{3}\pi R^3$$

Therefore, the density of the nucleus is approximately given as

$$\rho = \frac{\text{nuclear mass}}{\text{nuclear volume}}$$

$$\rho = \frac{m \times A}{V} = \frac{m \times A}{\frac{4}{3}\pi(1.2 \times 10^{-15})^3 \times A}$$

$$\rho = \frac{m}{\frac{4}{3}\pi(1.2 \times 10^{-15})^3} = \frac{1.66 \times 10^{-27}}{\frac{4}{3}\pi(1.2 \times 10^{-15})^3} = 2.29 \times 10^{17}\text{kgm}^{-3}$$

Thus, the nuclear density is nearly constant, independent of the atomic number and mass number. This characteristic, known as the saturation of nuclear density, is one of the most remarkable properties of atomic nuclei.

(iii) Threshold energy

The threshold energy is the excitation energy required to decompose the system into a specific decay channel. The decay process through which ^{12}C is formed via radiative capture of ^{8}Be and ^{4}He is shown in Fig.1.3. [2] In this figure, the second 0^+ state (7.65 MeV) is known as the Hoyle state. This state lies slightly above both the three-α decay channel and the ^{8}Be+^{4}He emission channel. Consequently, it can decompose not only through ^{8}Be+^{4}He emission but also via 3α decay channel.

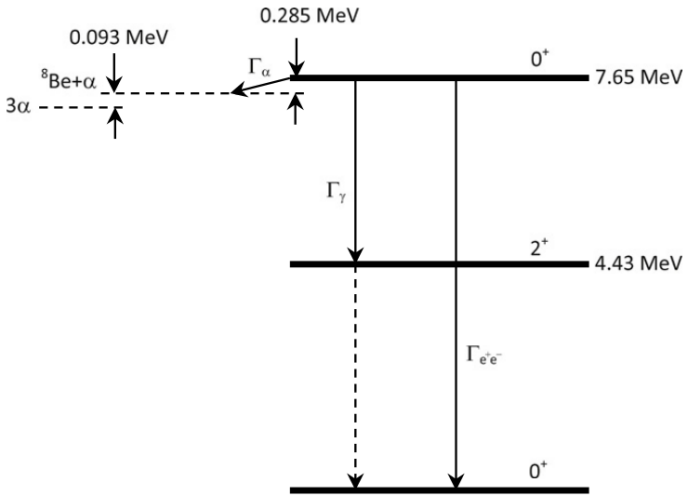

Figure 1.3: Schematic of the decay process by which ^{12}C is formed from the radiative ^{8}Be + ^{4}He capture

First, we consider the ^{8}Be+^{4}He threshold energy in a simplified way, which corresponds to the excitation energy required to decompose ^{12}C nucleus into ^{8}Be+^{4}He decay channel.

^{8}Be+^{4}He threshold energy=ground state energy of ^{8}Be+ground state energy of ^{4}He
+Kinetic energy between(^{8}Be+^{4}He) +Potential energy between (^{8}Be+^{4}He)

The kinetic energy between ^{8}Be+^{4}He is expected to be nearly zero in order to maintain the system with minimal relative momentum between them. Similarly, the potential energy between ^{8}Be+^{4}He is also approximately zero, since the two clusters will combine as the potential energy increases. This concept is known as the threshold rule, which is widely used in the study of nuclear clustering phenomena. Therefore, ^{8}Be+^{4}He threshold energy can be calculated as,

^{8}Be+^{4}He threshold energy=ground state energy of ^{8}Be+ground state energy of ^{4}He

The excitation energy required to decompose ^{12}C nucleus into ^{8}Be+^{4}He decay channel can be known by subtracting the ground state energy of ^{12}C to ^{8}Be+^{4}He threshold energy.

excitation energy from ^{12}C into ^{8}Be+^{4}He=92.1616-(28.2956+56.4992)=7.3668 MeV

The excitation energy of 7.3668 MeV is regarded as the threshold energy at which ^{8}Be+^{4}He decay cluster structure can form. When such a cluster- or molecule-like configuration emerges near the threshold energy (or near the height of the Coulomb barrier for heavier clusters), the inter-cluster wave function extends further outward, increasing the probability of the system residing in the peripheral region. Therefore, threshold energies serve as useful indicator for identifying the eigen energy states that exhibit cluster-type nuclear structure.

1.2 α Clustering

Nuclear clustering is the most unique and interesting phenomena observed in various physical aspects. The nucleus is a many-body quantum system composed of protons and neutrons, self-sustained by strong interaction, namely nuclear force. It often exhibits a remarkable tendency to form substructures, or clusters, within itself. To illustrate a full understanding of nuclear structure, the concept of nuclear clustering is crucial.

The distinct nature of nuclear forces against strong interaction between quarks and gluons can be realized in deuteron. It is the simplest bound two-nucleons system. The deuteron is only loosely bound with a 2.2 MeV binding energy and it exhibits no resonant state. This characteristic indicates that the nuclear force is short-ranged, spin- and isospin-dependent, and saturating in nature, allowing only a single weakly bound state for the proton–neutron pair. Nuclear force is strong enough to give strong binding effect when a nuclear structure formed from fragmented particles or clusters that are loosely compacted together. The existence of two kinds of fermions, protons and neutrons, is absolutely necessary for nuclear binding energy, as demonstrated by the strong binding force of the α-particle.

The α-particle (^{4}He nucleus) consists of two protons and two neutrons, forming a highly stable and tightly bound configuration. This stability arises from the Pauli exclusion principle, which prevents identical fermions from occupying the same quantum state. According to the binding energy per nucleon diagram, the binding energy of ^{4}He, ^{12}C, ^{16}O, ^{20}Ne and ^{24}Mg highlights the exceptional stability in low mass number region. Among these, the ^{4}He or α particle is considered as a well-established sub-unit of the nuclear structure. The alpha-like four-body correlations arise from the strong attractive correlation among four nucleons coupled each other in the relative S-state. Thus, nucleus can gain more binding energy by forming α-cluster itself as a fundamental building block in cluster model of nuclei inside the nucleus.

The nuclear shell model was proposed by M. G. Mayer [3] and O. Haxel et al., [4] within the framework of a single-particle potential that includes effective two-body correlations among nucleons. Shell model provides valuable information about in especially low-lying states because the single-particle field is always stable and essential correlations are predominantly of the two-body type. However, it fails to explain phenomena like collective behavior such as deformations, vibrations, rotations and excited nuclear states in many nuclei. This framework cannot fully describe phenomena where multi-nucleon correlations play a significant role. Therefore, alpha-cluster model in nuclei is a new window for investigating nuclear structure from different point of view.

In order to reveal a basic viewpoint of the cluster correlation and molecule-like structure in nuclear system, the research project on Alpha-Like Four Body Correlations and Molecular structure in Light Nuclei was organized by RIFP in 1976-1978. [5] This project aims to advance actively the comprehensive study of light nuclei based on the molecular viewpoint. They made cluster model calculations from He or Li region to Ne or Mg region in fairly wide range of excitation energy to confirm the appearance of various kind of molecule-like structures. The molecule-like structures are clearly observed in excited states of these α-nuclei of such as 3α in ^{12}C, ^{12}C+α in ^{16}O and ^{16}O+α in ^{20}Ne. Similar molecule-like states were also expected in ^{24}Mg. ^{24}Mg was expected the lightest nucleus that has the degree of freedom of relative motion between α-nuclei which mean the existence of the di-nuclear molecule-like structure composed of two α-nuclei ^{12}C+^{12}C. The theoretical investigations have been performed ^{16}O+2α for ^{24}Mg and ^{12}C+2α for ^{20}Ne and so on.

The group of Hokkaido university (Hiura, Shimodaya, Tamagaki ,and Tanaka) performed theoretically analysis in Beryllium region (^{8}Be and ^{9}Be) at the beginning of 1960's [6]. They pointed out for understanding about molecular-orbital model of atomic nuclei, α-cluster excited states, and the development of the cluster-core potential model. The 2α cluster structure of ^{8}Be with the microscopic studies of $\alpha - \alpha$ interaction points out that the remarkable characteristic feature of strong internal cluster correlations and weak inter-cluster correlations. The internal binding of constituent clusters is strong as binding energy of helium nucleus and the inter-cluster interaction is weak in the region where saturated clusters maintain their identity approximately. The validity of the α-cluster structure in the Be-region have been confirmed.

To extend the picture of alpha-like four-body correlations, the first excited 0^+ state of ^{12}C at 7.65 MeV is a plausible explanation for indicating three α clustering structure. Motivated by the importance of the alpha-correlations in sd-shell nuclei, the ^{20}Ne has a long attracted attention because it occupies within the sd-shell region, a role analogous to that of ^{8}Be in the p-shell. In 1967, the group of Hokkaido University introduced an alpha-cluster plus ^{16}O-core model for describing ^{20}Ne. Within this framework, the second 0^+ state of ^{16}O were interpreted as a configuration composed of the ground state of ^{12}C plus α cluster. J. Hiura and collaborators demonstrated that the ground $K^\pi=0^+$ rotational band of ^{16}O*can be reproduced using an α-core effective potential containing a repulsive core and state-dependent attractive well [6]. Consequently, ^{20}Ne exhibits a predominantly alpha-clustered character and $^{20}\mathrm{Ne}(0_1^+)$ is well described by a $^{16}\mathrm{O}_{\mathrm{g.s}} + \alpha$ configuration.

As a forward step to understand on the fundamentals of the cluster correlation in non-α-nuclei, studies on the nucleon-α and deuteron-α interactions of non-α-nuclei had also been performed. A non-α-nucleus is composed of an α core nucleus and valence nucleons which are correlated with each other in terms of various clustering correlations. ^{9}Be presented as a prototype of the molecule-like structure in non-α-nuclei, and ^{10}Be (^{10}B) nuclei are extended to the extremely neutron-rich isotopes of Be. The α-nucleus-core can change its structure by the activation of the α-cluster degree of freedom and the valence nucleons undergo various cluster correlations. These are combined with characteristic features of realistic nuclear forces and also with the effect of the Pauli Principle acting in each situation and there appear multi-phasic features of the molecule-like structure which could not be seen for cases of α-nuclei.

To illustrate the various possible nuclear α-cluster configurations, in 1968, Ikeda and colleagues proposed that alpha cluster structures could exist in many nuclei and introduced the Ikeda diagram [7], as shown in fig. 1.4. The diagram indicates the expected threshold energies required for breakup into different fragments and led to the hypothesis that the cluster states are likely to appear at excitation energies near these threshold energy. This concept is known as the Ikeda threshold rule.

The threshold energy associated with a particular cluster configuration in the Ikeda diagram can be obtained from nuclear binding energies. For example, the ground state binding energy of ^{16}O is equal to 127.61 MeV. To determine the threshold energy of ^{12}C+α configuration, the total binding energies of the two fragments in their ground states are

$$\mathrm{E}(^{12}\mathrm{C}+\alpha)=\mathrm{B}(^{12}\mathrm{C})+\ \mathrm{B}(\alpha)$$

where B(^{12}C)+ B(α) are the ground-state binding energies of ^{12}C(92.161620 MeV) and the α particle(28.29566 MeV), respectively. However, the kinetic energy between ^{12}C and α is nearly zero because momentum between ^{12}C and α need to be small value. And, also potential energy between ^{12}C and α is nearly zero for stability of cluster structure.

The threshold energy for the appearance of the ^{12}C and α in ^{16}O is then obtained by comparing the total binding energy of the compound nucleus with that of the separated fragments:

$$\mathrm{E}_{th}(^{12}\mathrm{C}+\alpha)=\mathrm{B}(^{16}\mathrm{O})\text{-}[\mathrm{B}(^{12}\mathrm{C})+\ \mathrm{B}(\alpha)]$$

A positive value of E_{th}(7.15272 MeV) indicates that the cluster configuration lies above the ground state of ^{16}O and therefore may manifest as an excited cluster state near that energy.

Similarly, the 3α breakup threshold energy in ^{12}C is determined by comparing the ground-state binding energy of ^{12}C with the total binding energy of three α particles. The resulting threshold energy is about 7.27 MeV. This procedure applies similarly to all other fragmentation's shown in the Ikeda diagram and forms the basis of the Ikeda threshold rule, which states that cluster states tend to appear at excitation energies close to their corresponding breakup threshold energies.

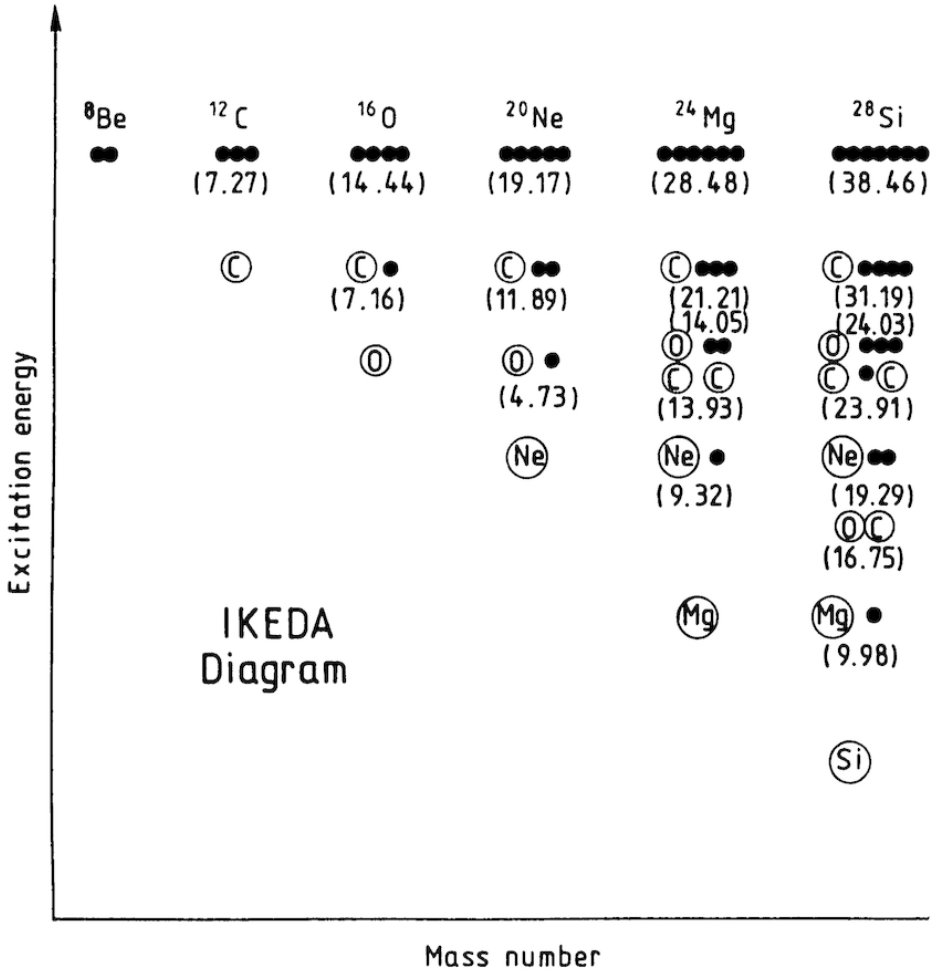

Figure 1.4: Ikeda diagram

One of the key quantities related to the structure-change is the dissociation (break up) threshold energy into the constituent clusters. Because nuclei with saturating properties tend to form fragment that are saturate, the dissociation energy for breaking a nucleus into several such clusters is relatively small. As a result, the molecule-like structure can appear near the threshold energy with only a small input energy. The existence of it near the threshold energy indicates that the binding energy of the inter-cluster relative motion is almost zero or positive.

In Ikeda diagram, the 3α threshold energy in ^{12}C appears at 7.27 MeV, while the 4α threshold energy in ^{16}O is shown at 14.44 MeV, with similar representations for heavier systems. These configurations are often illustrated as linear molecular states, however, they should not be interpreted as strictly linear configuration. For example, the Hoyle state in ^{12}C, with excitation energy of 7.656 MeV, is better described as a dilute, loosely bound 3α structure rather than a strictly linear chain structure. In heavier nuclei, the Nα molecular degrees of freedom emerge only at relatively high excitation energies within the diagram, reflecting the increasing complexity and reduced stability of such cluster configurations.

The Ikeda diagram also suggests an assumption that multiple nuclear configurations can coexist within the same nucleus. In the case of the ground state of the usual nuclei in which nucleons arrange in a spatially compact configuration, Pauli principle performs as a healing function to the orbital of shell models and brings about the independent-particle aspect. However, in the case of cluster molecule-like structure case, Pauli principle acts as an effective repulsive core force in the overlapping region of two α-nuclei and plays a role to sustain the molecule like structure through strengthening the characteristics of the clustering correlations. These distinctive functions of the Pauli principle in two different kinds of structure (or phase) were called as the "dual roles of the Pauli principle" [8].

For instance, in ^{16}O, the ground state is well described by a shell-model structure. In contrast, several excited states in the 6-10 MeV region exhibit as α+^{12}C cluster configurations, while states around 15 MeV are associated with a 4α cluster structure. Similarly, in ^{20}Ne, the first 0^+ excited state at 4.73 MeV is interpreted as a ^{16}O core nucleus plus α cluster. The third 0^+state at 11.89 MeV is described by a ^{12}C core with two additional α structures(^{12}C+$\alpha + \alpha$).

The Ikeda diagram provides a comprehensive framework for understanding not only the structural evolution between the shell-model-like and molecule-like configurations, but also the transitions between different types of molecule-like structure in α-conjugate nuclei. This is particularly valuable in the low excitation energy region up to 10 to 15 MeV, where such cluster structures are most prominent. It also mentions about the

structure-change of nuclear systems and the dominance of the alpha-correlation in light nuclei. The Ikeda diagram has been an analytical approach for both experimental and theoretical works on clustering in nuclei. It can indicate the range of excitation energies region in the experimental side where particular cluster structure might be expected to occur.

α clustering is an interesting subject in unusual nuclear phenomena in the nuclear region of N=Z nuclei such as Be, C, O, Ne, and so on. When the clustering correlation becomes so strong, the relative motion between clusters becomes the fundamental mode of motion of the nucleus. An extensive development of study of bound, quasi-bound and resonance levels of light nuclei has been promoted since there are possibility to appear α-particle molecule-like structure in wide region of nuclei both in mass number and in excitation energy. There are a lot of challenges upon variety of the molecule-like structure in excited states, structure-change between different kinds of structure, relation between cluster structure and the inter-cluster interaction, the independence of the cluster model and the accompanying effective two-nucleon interaction. Alpha clustering in nuclei is important in investigation of the change of nuclear structure formation, growth, breakup and fusion of clusters.

1.3 Alpha condensation

In addition to the relevance of the α-like four-nucleon correlations in atomic nuclei , two conceptually more challenging questions arise dealing with the α-clustering phenomena. The first concerns the competition between effective bosonic character of alpha cluster and underlying fermionic nature of its constituent nucleons. The second is whether the α-cluster states in nuclei may appear, such as interpretation as an α-condensate states, analogous to the Bose-Einstein condensation observed in finite systems of bosonic atoms such as Rb or Na confined in traps under specific conditions.

First of all, Satyendra Nath Bose and Albert Einstein theoretically predicted Bose-Einstein condensate in the mid 1920s. A Bose-Einstein condensate (BEC) is a state of matter that occurs when a collection of bosons is cooled to extremely low temperatures, very close to absolute zero(0 K or -273.15 °C). The first experimentally observation of Bose-Einstein condensate (BEC) in a dilute atomic vapor was announced by June, 1995 [9]. The first BEC was produced by E. A. Cornell and C. E. Wieman using rubidium-87 atoms at the University of Colorado Boulder. And, W. Ketterle also created another BEC using sodium atoms at MIT. All three received the 2001 Nobel Prize in Physics for this achievement. The evolution of Nα clustering structure around the thresholds for Nα breakup of α-conjugate nuclei in Ikeda diagram, leads to find the nα condensate state in α-conjugate nuclei.

As the first candidate of alpha condensate in finite nuclear system, ^{12}C is in highly interest. In 1954, F. Hoyle analyzed the synthesis of elements from carbon to nickel through nuclear reactions occurring in very hot stars. To explain the stellar abundance of carbon, he proposed the existence of the state composed of three-α clusters rather than individual nucleons [10]. To understand the properties of Hoyle state, its radius and excitation energies have been focused both experimental and theoretical studies.

The synthesis of ^{12}C in the helium burning phase proceeds through the triple-α process [11, 12]. According to the reaction sequence,

$$\alpha + \alpha + \alpha \rightarrow^{8} \mathrm{Be} + \alpha \rightarrow^{12} \mathrm{C}^{*}$$

the existence of the Hoyle state is significant in the stellar production of carbon in the universe. First, two α particles fuse to form ^{8}Be, which exists only in a short-lived equilibrium concentration. A third α particle can then be captured by ^{8}Be to form ^{12}C.

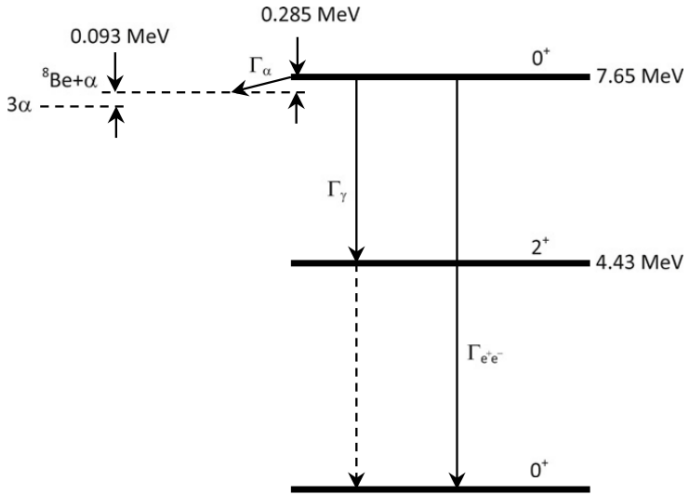

Figure 1.5: Schematic of the decay process by which ^{12}C is formed from the radiative ^{8}Be + ^{4}He capture

The capture of the α particle by ^{8}Be proceeds via tunneling through the Coulomb and centrifugal barriers. For s-wave capture, the centrifugal barrier vanishes, maximizing the probability of forming ^{12}C. Hoyle predicted the existence of a state at an excitation energy 7.65 MeV in which three α particles occupy the same 0s orbital with a spatially extended distribution. This Hoyle state is considered to be a phase transition namely 3α Bose-Einstein condensate and its remarkable structure has attracted significant theoretical and experimental interests for many years.

E. Uegaki et al. investigated the dynamical properties of 3α particle system microscopically by using the Resonating Group Method (RGM) [13]. They analyzed α-decay properties of $0_2^+, 2_2^+, 0_3^+, 2_3^+, 4_2^+$ and 3_1^+ by using the separation energy method and to clarify nuclear structure of excited states in this energy region of ^{12}C. They found anomalously large radius for the first excited 0^+ state which indicating a dilute, cluster-like structure to identify as the Hoyle state. The excited positive-parity levels at 7.7 MeV and 10.3 MeV in ^{12}C nucleus are well known for their anomalously large α-decay widths.

Subsequently, M. Kamimura calculated all multipole transition densities among seven T=0 states in ^{12}C by using the microscopic 3α resonating-group wave functions of the resonating group method(RGM) [14]. The transition densities between $0_1^+, 2_1^+, 0_2^+$ and 2_2^+ states revealed the transitions between the shell-like configurations and the molecule-like configurations involving significant spatial structural changes. R. Bijker and F. Iachello proposed that ^{12}C exhibits triangular α-Cluster symmetry, as three α's at the vertices of equilateral triangle, was performed [15]. They calculated electromagnetic transition strengths between ground state and Hoyle state, and successfully described the rotational-vibrational spectrum. And, they also attempted studies of cluster structure of light nuclei

within the framework of both the algebraic cluster model (ACM) for nα nuclei and the cluster shell model (CSM) for nα nuclei plus additional nucleons [16].

The α particle condensation aspect of the Hoyle state has been investigated theoretically using Tohsaki-Horiuchi-Schuck-Ropke (THSR) wave function [17]. The root-mean-square radius of the Hoyle state is calculated as 3.83 fm, whereas that of the ground state is 2.40 fm. Thus, the volume of the Hoyle state is three to four times larger than that of the ground state. They highlighted the Hoyle state as a prototype of α-cluster condensation in finite nuclei.

Single-α orbits and occupation numbers in eigen states of ^{12}C are investigated by T. Yamada and P. Schuck using the semi-microscopic 3α cluster model [18]. According to the alpha particle distribution in the Hoyle state as shown in Fig. 1.6, more than 70 percent of the alpha particles occupy in the lowest 0s state [19]. At densities lower than the nuclear saturation density and at low temperatures, α clustering is expected to dominate dilute symmetric nuclear matter. Therefore, the Hoyle state can be expressed as a condensate-like configuration in which the three-α-particles occupy identical lowest 0s state.

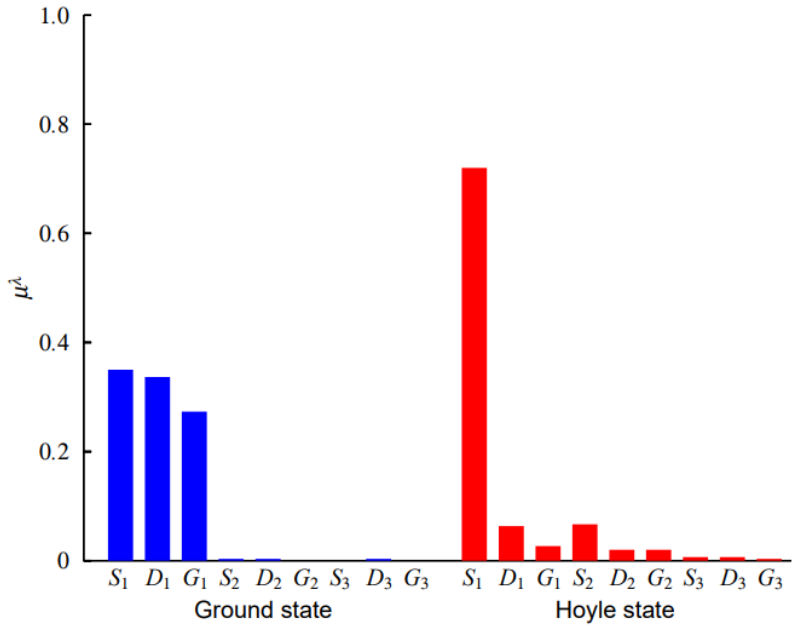

Figure 1.6: α particle occupation numbers in the ground state(left) and in the Hoyle state(right)

It has been widely argued that the Hoyle state can be regarded as a Bose-Einstein condensate(BEC) of α particles, similar to the Bose-Einstein condensation observed in finite trapped bosonic atoms such as Rb or Na. A. Tohsaki et al. [20] proposed new α cluster wavefunction to describe an α-particle condensed state where nα particles occupy the same 0s harmonic oscillator orbit. They performed generator coordinate method (GCM) calculations of ^{12}C and ^{16}O and compared their results with experimental data, as shown in Fig. 1.7.

For ^{12}C, the lowest calculated energy state(k=1), -85.9 MeV, is still above the observed binding energy of ^{12}C (-92.16 MeV). This indicates that the functional space used in the calculation is not sufficiently large to fully reproduce the system. The calculated root-mean-square radius is also slightly greater than that of experimental data(2.65 fm). The calculate rms radius of second 0^+ state (k=2), 4.29 fm is much larger than that of ground state, 2.97 fm. Therefore, the second 0^+ state corresponds to a very dilute system of average density.

TABLE I. Comparison of the generator coordinate method calculations with experimental values. $E^{\rm thr}_{n\alpha} = nE_\alpha$ denotes the threshold energy for the decay into α clusters; the values marked by * correspond to a refined mesh (see main text).

		E_k (MeV)	$E_{\rm exp}$ (MeV)	$E_k - E^{\rm thr}_{n\alpha}$ (MeV)	$(E - E^{\rm thr}_{n\alpha})_{\rm exp}$ (MeV)	$\sqrt{\langle r^2\rangle}$ (fm)	$\sqrt{\langle r^2\rangle}_{\rm exp}$ (fm)
^{12}C	$k=1$	-85.9	-92.16 (0^+_1)	-3.4	-7.27	2.97	2.65
	$k=2$	-82.0	-84.51 (0^+_2)	$+0.5$	0.38	4.29	
	$E^{\rm thr}_{3\alpha}$	-82.5	-84.89				
^{16}O	$k=1$	-124.8 (-128.0)*	-127.62 (0^+_1)	-14.8 (-18.0)*	-14.44	2.59	2.73
	$k=2$	-116.0	-116.36 (0^+_3)	-6.0	-3.18	3.16	
	$k=3$	-110.7	-113.62 (0^+_5)	-0.7	-0.44	3.97	
	$E^{\rm thr}_{4\alpha}$	-110.0	-113.18				

Figure 1.7: Comparison of the generator coordinate method calculations with experimental values.

After an active search for the 3α condensate in ^{12}C [21, 22], the alpha condensate state in ^{16}O assume as a next target. Oxygen nucleus was discussed as the next candidate for the α-condensate as the same way. The calculated rms radius of ($0^+_{k=1}$) state in ^{16}O, 2.59 fm, is slightly smaller than experimental result(2.73 fm). And, the second ($0^+_{k=2}$) state is bound by 6 MeV below the theoretical 4α threshold energy. This state is argue that there will be some mixing between its and the ^{12}C+α state. The third ($0^+_{k=3}$) state is bound 0.7 MeV below the 4α threshold energy and its rms radius is 3.97 fm. According to this dilute density, the author expected that it should be considered as just 4α-cluster condensed state.

The 0^+ spectrum of ^{16}O has very well produced with semi-microscopic cluster model, α+^{12}C OCM (Orthogonality Condition model), as shown in Fig. 1.8. [23]. Two kinds of effective two-body nucleon-nucleon forces MHN(Modified Hasegawa-Nagata) and SW(Schmidt-Wildermuth) are adopted. There are several 0^+states interpreted as an α+^{12}C cluster configuration between the 4α threshold and the ground state. Six calculated 0^+states are well converged with experimental result. With the two different effective $\alpha - \alpha$ forces, they can reproduce the full spectrum of 0^+ states and tentatively make a one-to-one correspondence of those states with the experimental spectrum.

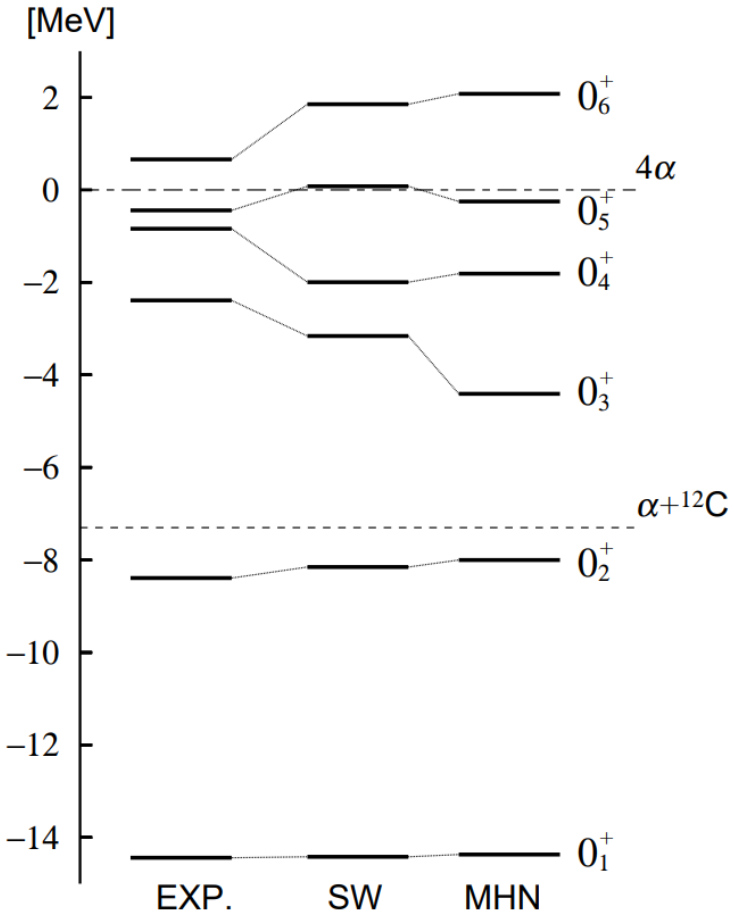

Figure 1.8: Comparison of energy spectra between experiment and the present calculation. Two kinds of effective two-body nucleon-nucleon forces MHN and SW are adopted. Dotted and dash-dotted lines denote the α+^{12}C and 4α thresholds, respectively

The alpha condensate state in ^{16}O may be more complicated than in ^{12}C, even in the 0^+ channel. Exciting one α particle out of the ground state in ^{12}C, all three α's form the gas state(3α condensed state). However, exciting one α-particle out of the ground state of ^{16}O, may leave the remaining ^{12}C core nucleus either in its ground state or in various excited states of the shell model type rather than immediately forming a dilute α gas(4α condensed state). In order to obtain the α gas state in ^{16}O, at least two α's 'knock loose' are really important.

Another theoretical study was performed to analyze energy spectrum of 0^+ states in ^{16}O from the OCM (Orthogonality condition model) and THSR approaches. There are several 0^+states interpreted as an α+^{12}C cluster configuration between the 4α threshold and the ground state as shown in Fig. 1.9 [19]. Six calculated 0^+states are good in correspondence between experimentally and two different theoretical approaches each other.

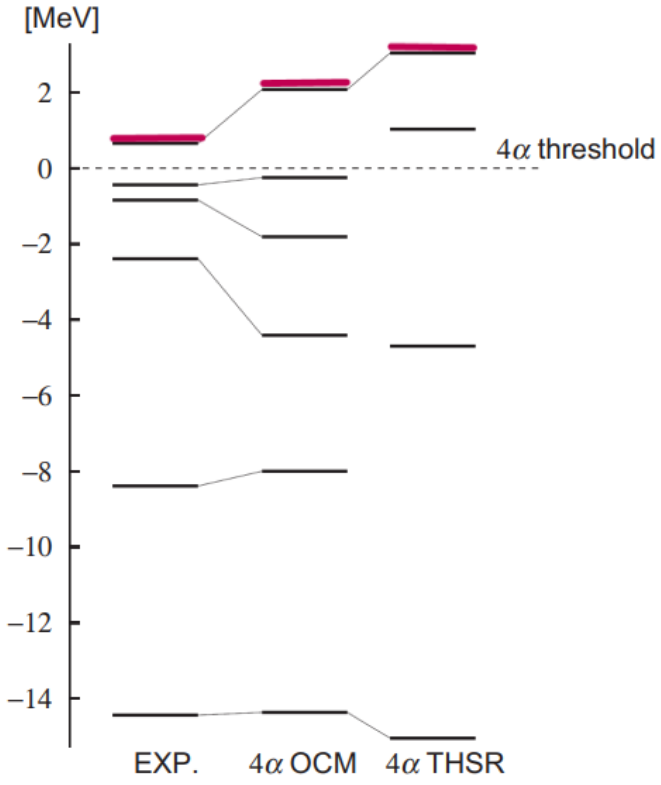

Figure 1.9: Spectrum of 0^+ states in ^{16}O from the OCM and THSR approaches

The 0^+_6 state of ^{16}O at E_x=15.1 MeV is identified from a theoretical analysis as being a strong candidate of a 4α condensate [24]. The highest red lines are represented as α condensate states of theoretical and experimental sides respectively. The other four excited states are supposed to have α+^{12}C configurations, for example, the 0^+_5 state ,

below the highest state, is interpreted as an α orbiting in a higher nodal S-wave around the ground state of ^{12}C. The 0_4^+ state is expressed as α orbiting in a P-wave around the first 1^- state in ^{12}C. [25] In the 0_3^+, the α is in a D-wave coupled to the 2_1^+ state of ^{12}C. The second 0^+ state, the α is in a 0s-wave and the ^{12}C in its ground state. The THSR approach, the dominant framework for studying α condensation, could reproduce correctly the ground state and the α condensate state 0_6^+.

The interest of the α condensate in ^{20}Ne and heavier nuclei has been increasing. In order to search for the 5α condensed state in ^{20}Ne, the excitation energy spectrum of $^{20}\mathrm{Ne}(\alpha, \alpha' + \alpha)\ ^{16}\mathrm{O}(0_6^+)$ reaction was measured at the Research Center for Nuclear Physics (RCNP), Osaka University [26]. In Fig. 1. 10, the newly observed states at E_x =23.6, 21.8, and 21.2 MeV in ^{20}Ne are strongly coupled to the 0_6^+ state in ^{16}O and it is proposed as a candidate for the 5α condensed state.

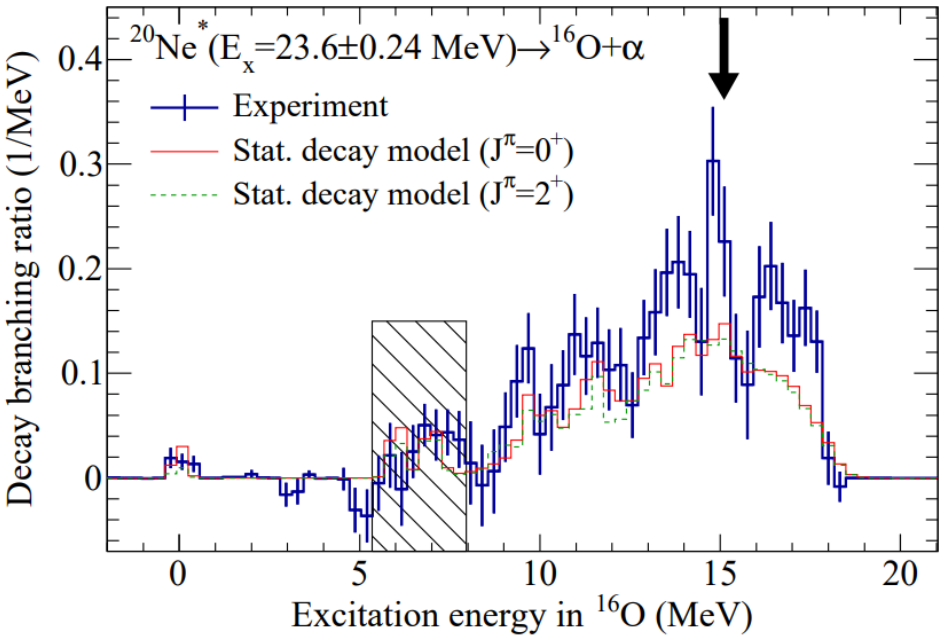

Figure 1.10: Decay branching ratio of the excited state in ^{20}Ne at E_x = 23.6 ± 0.24 MeV populated by the inelastic alpha scattering at 0 degree (thick blue solid lines with error bars) compared with the statistical-decay-model calculations from the isoscalar 0^+ and 2^+ states in ^{20}Ne (thin red solid and green dashed lines). The dead layers of the Si detectors caused the uncertainty on the kinetic energies of alpha particles in the hatched area.

B. Zhou et al., [27] performed prediction about 5α condensate in ^{20}Ne as a first theoretical evidence by using THSR wave function. Two 0^+ eigen states are obtained and one eigen state around 22 MeV is a strong candidate for 5α condensate state that could be the 5α state observed in recent experiment.

The 6α-condensed state in ^{24}Mg has been searched by measuring the ^{12}C+^{12}C scattering with the SAKRA Si detector array at E_{cm}=17.5-25.0 MeV. The inclusive cross sections for the reactions peaked at E_{cm}=19.4 MeV,

$$^{12}\mathrm{C} + ^{12}\mathrm{C} \rightarrow ^{12}\mathrm{C}(0_2^+ \mathrm{or} 3_1^-) + X \rightarrow 3\alpha + X$$

which corresponds to the excitation energy of 33.3 MeV in ^{24}Mg [28]. This 19.4 MeV state actually couples with the 0_2^+ as the 3α-condensed state, and its energy is close to the theoretical value of the 6α-condensed state. They suggest that this state is a candidate for the 6α-condensed state by experimentally. It is essential to compare with theoretical calculations. Therefore, theoretical efforts are strongly desired to establish the 6α-condensed state.

At present, the formation of α condensates is in much interest in strongly coupled fermionic systems. According to many theoretical results, α clusters might condense at the same lowest 0s orbit in their common mean field at low densities and temperatures due to their bosonic nature. The prospects of α condensate states in ^{12}C, ^{16}O and ^{20}Ne are expressed. Further experiments and various theoretical methods upon various candidate nuclei are necessary in order to illustrate the Alpha Condensate situation.

1.4 Alpha Condensation with the core nucleus

When several authors have discussed the possibility of α-particle condensation in low density nuclear matter, there existed an ambiguous problem that what is the maximum number of alpha clusters for multi-alpha condensed state and how will these multi-clusters manage to overcome the instability situation in heavy nuclear systems. As a schematically illustrated in the Ikeda diagram, nα condensates are generally expected to appear at significantly higher excitation energies relative to the ground state of the composite system. This poses a substantial challenge for their experimental observation.

As an analysis of maximum number of alpha clusters in multi-alpha condensed state, in 2004, a newly proposed α-cluster wave function based on the GrossPitaevskii-equation together with the Hill-Wheeler equation was applied to the dilute Nα states of nuclei from ^{12}C to ^{40}Ca with $J^{\pi} = 0^{+}$, in the excitation energy region from threshold up to about 20 MeV [29]. The aim of this theoretical work was to investigate dilute multi-α cluster condensed states with spherical and axially deformed configurations, and to determine the maximum number of α clusters for multi-α condensed state. α-condensates can be analyzed roughly by calculating using the known alpha-alpha potential with a self-consistent approach. And, alpha condensate will have Coulomb barriers for the decay into multiple α's.

As shown in Fig. 1.11, the Nα cluster states become unstable as the Coulomb repulsion (mentioned as a dotted line) increases depending on the number of α particles. By comparing single-α particle potentials U(r)-solid line for 3α, 4α, 5α, 8α and 10α, the potential depths are getting shallower with increasing number of α clusters, mentioned reducing stability. And, the Coulomb barrier also getting larger with number of α clusters to force to be strong repulsion between clusters. Based on the analysis of the properties of these dilute Nα systems, the maximum number of α particles capable of forming a self-bound nucleus is reported to be approximately ten. According to the result, the heaviest nucleus is estimated to be around ^{40}Ca.

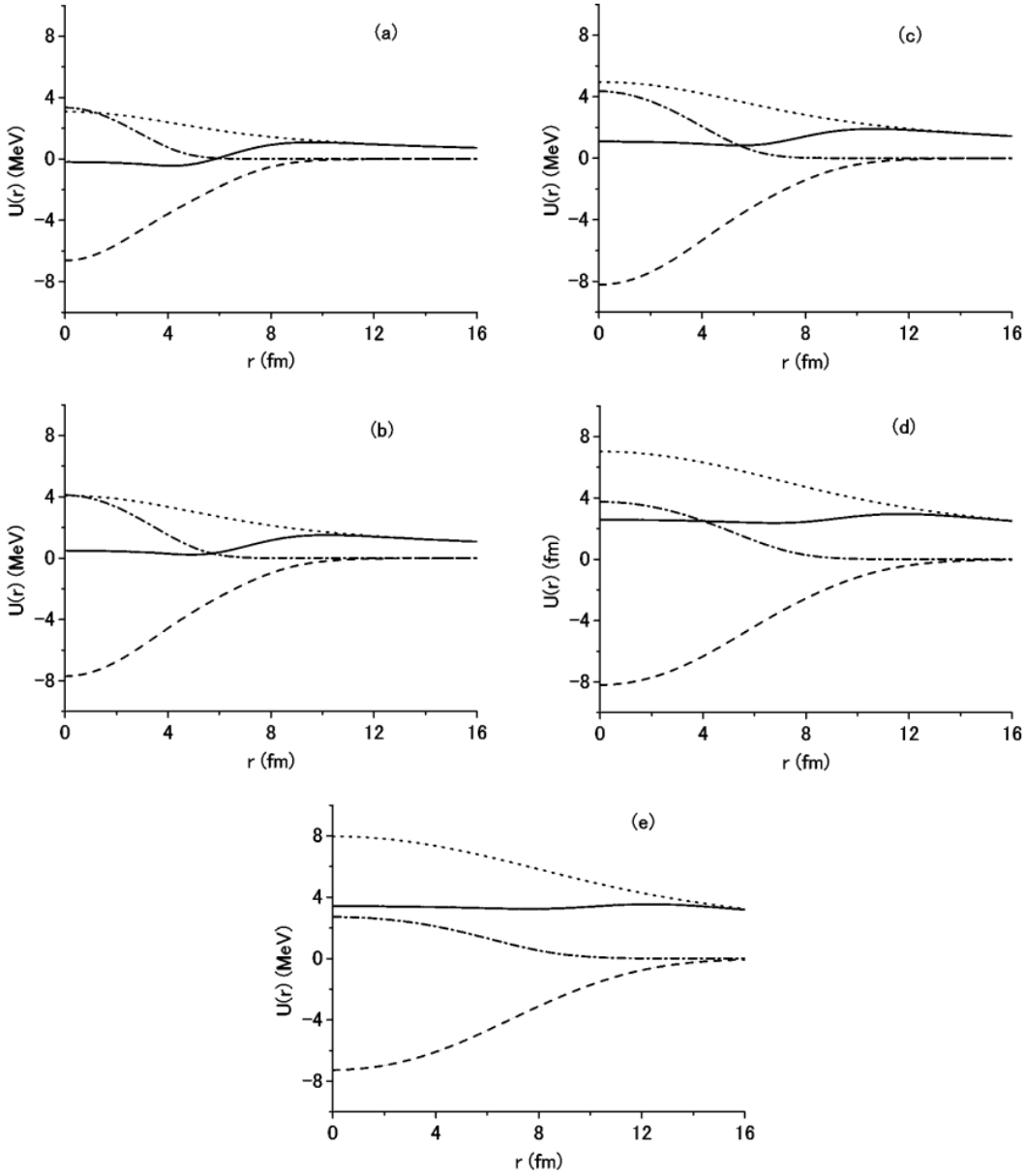

Figure 1.11: Single-α-particle potentials U(r) (solid line) which are obtained by solving the Gross-Pitaevskii equation with the density dependent potential; (a) 3α, (b)4α, (c) 5α, (d) 8α, and (e) 10α systems. the dashed, dot-dashed, and dotted lines demonstrate, the contribution from the two-range-Gaussian term, density-dependent term, and Coulomb potential respectively.

In 2005, γ-ray spectroscopy in coincidence with the emission of ^{8}Be and ^{12}C$^{*}(0_2^+)$ from a compound nucleus has been conducted by using the following reactions [30]. ^{18}O+^{13}C$\rightarrow^{31}$Si$\rightarrow^{23}$Ne+^{8}Be and ^{28}Si+^{24}Mg$\rightarrow^{52}$Fe$\rightarrow^{40}$Ca+^{12}C$^{*}(0_2^+)$. They interested in the coherent multiple α-particle emission from excited compound nuclei.

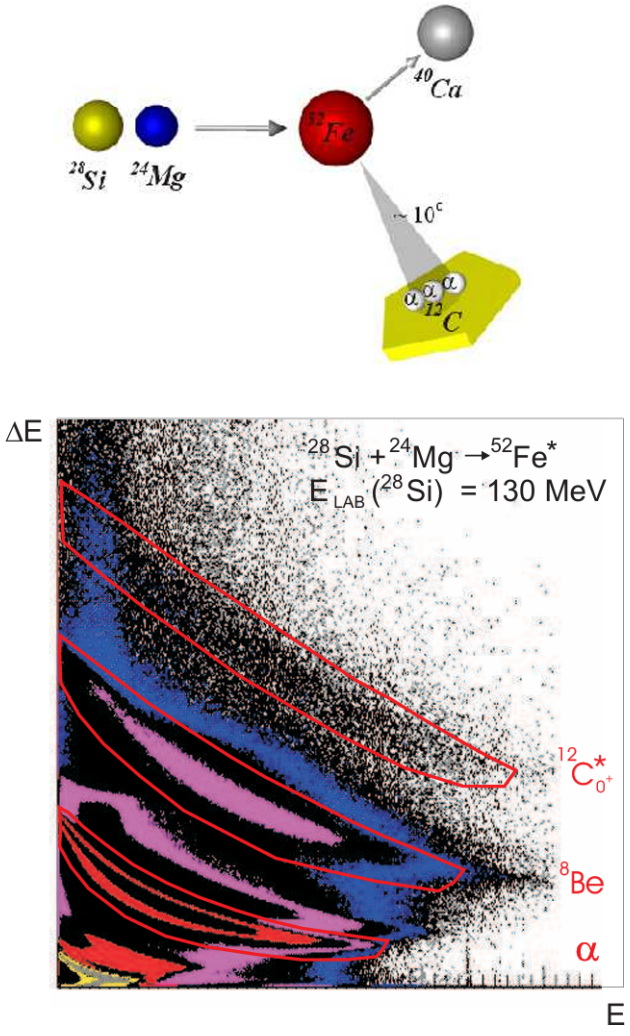

Figure 1.12: Top: This part shows the kinematical situation for the triple pile-up of the signals for 3α's in one detector and the emission cone for α's form the decay of ^{12}C$^{*}(0_2^+)$. Bottom: Plot of δE-E-signals as observed with the ISIS charged particle detector system. This events with the emission of single α's, of ^{8}Be and with three α's from the state ^{12}C$^{*}(0_2^+)$ are indicated. The reaction is ^{28}Si+^{24}Mg$\rightarrow^{52}$Fe$\rightarrow^{40}$Ca+X at E-lab=130 MeV (courtesy of Tz. Kokalova).

It can be considered that the emitted second 0^+ state of ^{12}C and the ground state of ^{8}Be are formed inside the Coulomb barrier of the compound nucleus. The data point out clearly experimental features for the existence of Bose-Einstein condensates in nuclei giving rise to coherent multi α-particle states in excited N=Z nuclei. These experimental evidences point out a hypothesis that α-condensed state may be formed not only in ^{8}Be and ^{12}C but also in heavier nuclei with some core nucleus. The presence of a core nucleus can potentially assist the formation of α condensates at relatively small excitation energies through attractive core-α interaction and the Coulomb barrier. This core+nα condensate is a more accessible pathway for experimental exploration, although such candidates have not yet been firmly identified experimentally.

In the Ikeda diagram, the α-condensation hypothesis proposed that, at certain excitation energies near the multi-α decay thresholds, a nucleus may take the form of a compact core such as a tightly bound cluster, ^{12}C or ^{16}O, and surrounded by loosely bound α particles, which can occupy a common low-density, gas-like configuration analogous to a Bose-Einstein condensate. A possible solution to the instability problem of multi-α-condensed state is to assume the presence of the core nucleus that provides an additional attractive potential for the surrounding α-clusters. The possibility of α condensed states forming around a core nucleus in heavier nuclei is therefore an important subject to be investigated.

The first theoretical examination of above hypothesis was carried out using the Virtual Schuck Wave function, a Monte Carlo technique designed to describe the Schuck-type wave function that has been successfully applied to the α-condensed Hoyle state [31]. The α-condensed state in ^{12}C is well-expressed within this framework by analyzing relevant physical quantities such as energy convergence of ^{12}C measured from the $\alpha + \alpha + \alpha$ threshold and root-mean-square radius. The study of situation of alpha-condensate in non-4N-nuclei was rather easy to extend by using these virtual Schuck approach. The possibility of a condensed state consisting of α and dineutron clusters, ^{10}Be, was investigated because dineutron correlation is also important in weakly bound neutron-rich nuclei.

As an extension to the system with a core, the 2α-condensed state around the ^{16}O core in ^{24}Mg and 3α-condensed state around the ^{16}O core in ^{28}Si have also been investigated. [31] These α-condensed configurations in ^{24}Mg and ^{28}Si can be realized by appropriately adjusting the proper values of the oscillator parameter associated with the α-condensate.

And also, N. Itagaki et al., [32] analyze the three α state around ^{40}Ca based on a microscopic α-cluster model. They introduced Virtual THSR wavefunction and predicted three α cluster configuration around ^{40}Ca. The calculated three α cluster state around ^{40}Ca appeared below the top of Coulomb barrier when its spatial extension was comparable with that of a famous Hoyle state. By comparing threshold energies between ^{40}Ca+3α and ^{40}Ca+α, forming three α clusters simultaneously need more than triple energy than adding single α cluster. The kinetic energy between core and each α cluster is about 20 MeV, Pauli principle between nucleons in the core and α cluster strongly effect in nuclear structure. They concluded that tripleα+^{40}Ca core is likely to be stable according to their results.

The identification of the molecule-like structure at high excitation energies, where various types of so-called molecular resonance appear, is more difficult than at the relatively low excitation energy region. This difficulty arises from the dense background of compound-nucleus levels and the existence of many open decay channels. In general, the emergence of molecule-like configurations in the excited states of nuclei reflects a structural-transition as a kind of phase change in the nuclear many-body system due to the clustering correlations.

The gas-like states composed of α clusters around a ^{16}O core in ^{24}Mg have been performed by Ichikawa et al. [33]. They performed generator coordinate method (GCM) with Brink-type cluster wavefunction. The basic consideration to identify gas-like states was that all of the α clusters occupied the same 0s orbital in the form of spatially extended distribution. The existence of such cluster structure is expected by the strong enhancement of isoscalar monopole (E0) transitions. The energies of the 0^+ states of ^{24}Mg measured from the ^{16}O+α+α threshold are calculated. Among them, they selected four eigen states (-8.01,-5.10, -1.67, 0.10) MeV as possible resonance states according to the energy convergence behavior as shown in Fig. 1.13 (yellow box).

TABLE I. The energies of the 0^+ states of ^{24}Mg measured from the $^{16}\mathrm{O}+\alpha+\alpha$ threshold (MeV) and squared overlap with the THSR wave functions for the two α clusters around ^{16}O (σ = 3, 4, 5, and 6 fm).

Energy (MeV)	$\sigma = 3$ fm	$\sigma = 4$ fm	$\sigma = 5$ fm	$\sigma = 6$ fm
−16.63	0.266	0.109	0.009	0.004
−9.99	0.000	0.000	0.000	0.000
−8.90	0.001	0.001	0.001	0.000
−8.01	0.124	0.074	0.059	0.024
−7.89	0.003	0.002	0.001	0.001
−7.17	0.000	0.000	0.000	0.000
−5.10	0.402	0.364	0.333	0.208
−2.66	0.000	0.000	0.000	0.000
−1.81	0.001	0.002	0.001	0.001
−1.67	0.043	0.061	0.037	0.030
−1.29	0.002	0.002	0.002	0.002
−0.11	0.000	0.001	0.001	0.002
0.10	0.001	0.004	0.008	0.019
0.43	0.000	0.001	0.001	0.002
1.51	0.039	0.111	0.115	0.103

Figure 1.13: The energies of the 0^+ states of ^{24}Mg measured from the $^{16}\mathrm{O}+\alpha+\alpha$ threshold (MeV) and squared overlap with the THSR wave functions for the two α clusters around ^{16}O (σ=3, 4, 5, and 6 fm).

They analyzed the strength distribution of the isoscalar E0 transition from the ground state to the four selected resonance states, as shown in Fig. 1.14. The result shows that the -5.10 MeV and -1.67 MeV eigen states are strongly excited by the E0 transition operator because of large components of gas-like cluster states. These two eigen states could be concluded as possible candidates of α gas-like states and could be observed from the experiment.

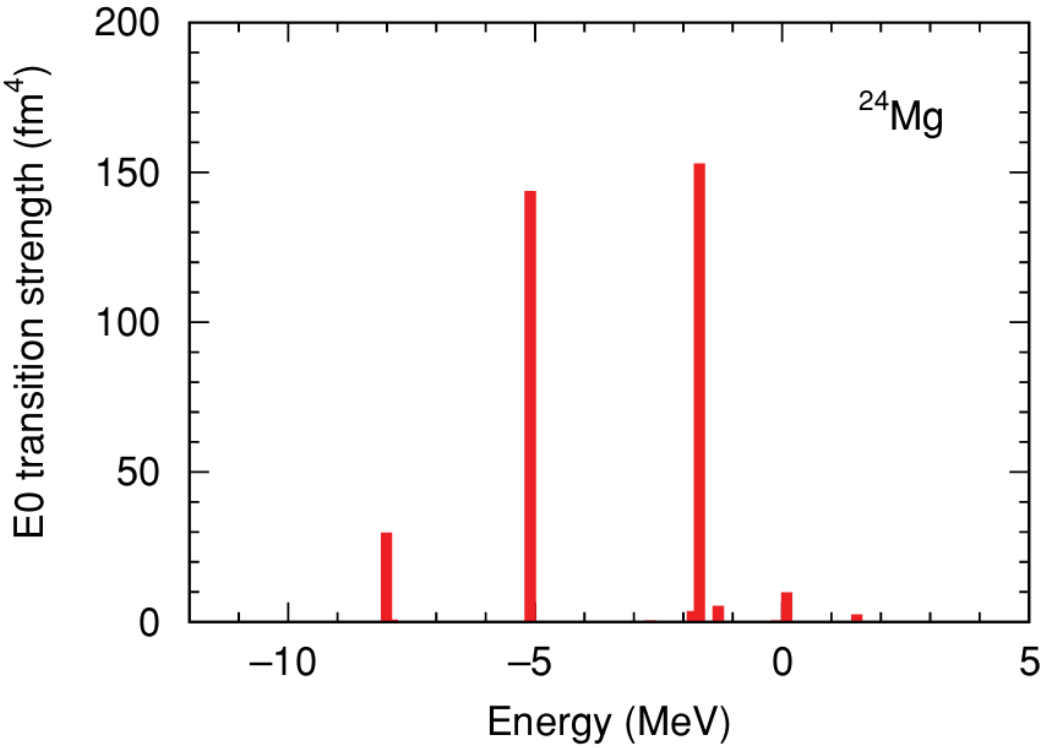

FIG. 2. (Color online) The strength distribution of the isoscalar $E0$ transition from the ground state (fm^4). Here the matrix elements of isoscalar $E0$ operator are squared. The energy is measured from the $^{16}\mathrm{O} + 2\alpha$ threshold.

Figure 1.14: (Color line) The strength distribution of the isoscalar E0 transition from the ground state (fm^4). Here the matrix elements of isoscalar E0 operator are squared. The energy is measured from the ^{16}O+2α threshold.

The α-condensate with the core nucleus opens a new window for the analysis of multi-α-cluster condensation in atomic nuclei. Many theoretical findings and experimental results are necessary for strong identification of the existence of the α-condensate with the core nucleus.

1.5 Motivation

As a reasonable solution to the instability of multi-α condensate, the presence of the core nucleus that supports an attractive potential started an active search. The presence of a core nucleus can potentially assist the formation of α condensates at relatively small excitation energies through attractive core-α interactions and the Coulomb barrier. This core+nα condensate is a more accessible pathway for experimental exploration, although such candidates have not yet been firmly identified experimentally.

Theoretically, Ichikawa et al. [33] have discussed the possible existence of ^{16}O+2α condensates through the calculation within the ^{16}O+nα model space. They discussed that these candidates (excited 0^+ states) are characterized by strong isoscalar monopole transition strengths, which serve as a signature for spatially extended cluster configurations. They used a method where the Hamiltonian was diagonalized by randomly generated α particle configurations. While this method provided valuable insights, the randomly generated wave functions include physically unimportant configurations, leading to a strong mixing of resonances and non-resonant states. Consequently, it was unclear which of the obtained eigen states were real resonances.

There was no clear evidence to point out α-condensation with the core nucleus. To address mentioned theoretical limitations and further investigations of the ^{16}O+2α condensate, we employ the real-time evolution method (REM) to describe the ^{16}O+2α system. It is a theoretical framework that utilizes the equation of motion (EOM) of Gaussian wave packets to generate basis wave functions. An advantage of REM is its ability to generate physically essential basis states with less contamination from the continuum. Furthermore, we estimate the α-decay width of the resonances by employing the analytical continuation in the coupling constant (ACCC). The discussion for calculated rms radius values and isoscalar monopole (E0) transitions for each α-condensed state should be included. My research provides a more robust examination of the predicted ^{16}O+2α condensation in ^{24}Mg.

Chapter 2

Theoretical Framework

In the theoretical framework chapter, there are four sub-sections, namely I. Hamiltonian and model wave function, II. Real-time evolution method, III. Calculation procedure and IV. Analytical continuation in the Coupling Constant(ACCC).

2.1 Hamiltonian and model wave function

The Hamiltonian and the model wave function used in our study are almost identical to those used by Ichikawa et al. [33]. The Hamiltonian for the Nα system is composed of the kinetic energy, the effective two-body nuclear interaction, and the Coulomb interaction.

$$\hat{H} = \sum_{i=1}^{4N} \hat{t}_i - \hat{t}_{cm} + \sum_{i<j}^{4N} \hat{v}_N(\boldsymbol{r_{ij}}) + \sum_{i<j}^{4N} \hat{v}_C(\boldsymbol{r_{ij}}) \tag{2.1}$$

where, $\hat{t}_i$ denotes the kinetic energies of the nucleons and $\hat{t}_{cm}$ is the center of mass kinetic energy which is exactly removed from $\hat{t}_i$. And, $\hat{v}_C$ is mentioned as the Coulomb interaction between protons.

The effective nuclear interaction $\hat{v}_N$ used in our study is the Volkov No.2 [34] effective nucleon-nucleon interaction with a slight modification [35] is used as follow.

$$\hat{v}_N(\boldsymbol{r_{ij}}) = (W - MP_\sigma P_\tau) \sum_{k=1,2} V_k \exp\{-(\frac{\boldsymbol{r}^2}{c_k^2})\} \tag{2.2}$$

where $P_\sigma P_\tau$ are spin and isospin exchange operators which exchange the position of proton and neutron and each proton can interact two neutrons and vice-versa, in α-particle. The Wigner parameter is set as W=1-M with the Majorana exchange parameter M=0.63. The other potential parameters applied in our calculation are V_1 =60.650 MeV, V_2 = -61.140 MeV, c_1 = 0.980 fm^{-2} and c_2= 0.309 fm^{-2}.

The model wave function for the ^{16}O+2α system is described by the Brink-Bloch wave function [36] composed of the ^{16}O core and two α clusters,

$$\Phi(\boldsymbol{z}_1, \boldsymbol{z}_2) = A\{\psi_\alpha(\boldsymbol{z}_1)\psi_\alpha(\boldsymbol{z}_2)\psi_O(\boldsymbol{z}_O)\} \tag{2.3}$$

where A is the antisymmetrization operator that exchanges the nucleons belonging to different clusters.

Each α cluster wave function $\psi_\alpha(\boldsymbol{z})$ describes four nucleons (two protons and two neutrons with spin up and down) in a $(0s)^4$ configuration.

$$\psi_\alpha(\boldsymbol{z}) = A\{\phi(\boldsymbol{r}_1, \boldsymbol{z})\chi_{p\uparrow}...\phi(\boldsymbol{r}_4, \boldsymbol{z})\chi_{n\downarrow}\} \tag{2.4}$$

where $\chi_{p\uparrow}$, etc., denote the spin-isospin states of the nucleons.

The single-particle wave function is defined by Gaussian form function as follows

$$\phi(\boldsymbol{r}, \boldsymbol{z}) = \left(\frac{2\nu}{\pi}\right)^{3/4} exp\{-\nu\left(\boldsymbol{r} - \frac{\boldsymbol{z}}{\sqrt{\nu}}\right)^2 + \frac{1}{2}z^2\} \tag{2.5}$$

Here, ν is the size parameter of the α particle, and is chosen to reproduce the observed radius of ^{4}He (ν=0.275 fm^{-2}).

The complex-valued three-dimensional vector $\boldsymbol{z}$ represents the center of the Gaussian wave packet in phase space, i.e., the real part of z coordinate represents the spatial position, and the imaginary part of z corresponds momentum of an α particle, respectively. The only difference between our study wave function and Ref. [33]'s lies in the Gaussian centroid, which is parametrized by real-valued or complex-valued three-dimensional vectors.

The ^{16}O cluster is approximated as a 4α system,

$$\psi_O(\boldsymbol{z}_O) = A\{\psi_\alpha(\boldsymbol{z}_3)...\psi_\alpha(\boldsymbol{z}_6)\} \tag{2.6}$$

$$\boldsymbol{z}_O = \frac{1}{4}(\boldsymbol{z}_3 + ... + \boldsymbol{z}_6) \tag{2.7}$$

where the centroids of four α particles $(\boldsymbol{z}_3 + ... + \boldsymbol{z}_6)$ are fixed at the vertex of a tetrahedron with a side length of 0.5 fm, and only their center-of-mass $(\boldsymbol{z}_O)$ is treated as a free parameter. Furthermore, we impose the condition that the center of mass of the system is located at the origin, i.e., $\boldsymbol{z}_1 + \boldsymbol{z}_2 + 4\boldsymbol{z}_O = 0$. Thus, the model wave function in Eq. (2.3) has two independent parameters, $\boldsymbol{z}_1$ and $\boldsymbol{z}_2$.

2.2 Real-time evolution method

Imai et al. [37] proposed the real-time evolution method (REM) for generating the basis wave functions by using the equation of motion (EOM) of the Gaussian wave packets. Real-time evolution method has a good opportunity for investigating the ground and excited cluster configuration of atomic nuclei. And also this method is relevant to more general cases such as non-α cluster wave functions, antisymmetrized molecular dynamics (AMD) and fermionic molecular dynamics (FMD) wave functions.

The most significant feature of our study is that the basis functions are generated by using the equation of motion (EOM), while they were generated stochastically (randomly) in Ref. [33]. We regard $\boldsymbol{z}_1$, $\boldsymbol{z}_2$ and $\boldsymbol{z}_O$ as the time-dependent parameters and derive the EOM from the time-dependent variational principle:

By applying the time-dependent variational principle to the intrinsic wave function given by Eq. (2.3),

$$\delta \int dt \frac{\langle \Phi(\boldsymbol{z}_1, \boldsymbol{z}_2) | i\hbar d/dt - \hat{\boldsymbol{H}} | \Phi(\boldsymbol{z}_1, \boldsymbol{z}_2) \rangle}{\langle \Phi(\boldsymbol{z}_1, \boldsymbol{z}_2) | \Phi(\boldsymbol{z}_1, \boldsymbol{z}_2) \rangle} = 0 \tag{2.8}$$

And derive the equation of motion(EOM) regarding $\boldsymbol{z}_1, \boldsymbol{z}_2$ and $\boldsymbol{z}_O$ as the time-dependent parameters.

$$i\hbar \sum_{j=1}^{2} \sum_{\sigma=x,y,z} C_{ip;j\sigma} \frac{dz_{j\sigma}}{dt} = \frac{\partial E_{int}}{\partial z^*_{ip}} \tag{2.9}$$

$$E_{int} := \frac{\langle \Phi(\boldsymbol{z}_1, \boldsymbol{z}_2) | \hat{\boldsymbol{H}} | \Phi(\boldsymbol{z}_1, \boldsymbol{z}_2) \rangle}{\langle \Phi(\boldsymbol{z}_1, \boldsymbol{z}_2) | \Phi(\boldsymbol{z}_1, \boldsymbol{z}_2) \rangle} \tag{2.10}$$

$$C_{ip;j\sigma} := \frac{\partial^2 \ln \langle \Phi(\boldsymbol{z}_1, \boldsymbol{z}_2) | \Phi(\boldsymbol{z}_1, \boldsymbol{z}_2) \rangle}{\partial z^*_{ip} \partial z_{j\sigma}} \tag{2.11}$$

Starting from an arbitrary initial wave function at t=0, we solve this EOM to calculate the time evolution of $\boldsymbol{z}_1$ and $\boldsymbol{z}_2$. As a result, the equation of motion (EOM) yields the time-dependent vectors $\boldsymbol{z}_1$(t) and $\boldsymbol{z}_2$(t). We expect that if time evolves long enough, the ensemble of the wave functions $\Phi(\boldsymbol{z}_1(t),\boldsymbol{z}_2(t))$ spans a good model space to describe both bound states and resonances.

The ensemble of the wave functions $\Phi(\boldsymbol{z}_1(t),\boldsymbol{z}_2(t))$ follows the quantum statistics [38]. If the nucleon emission process are properly treated, the ensemble of the wave functions $\Phi(\boldsymbol{z}_1(t),\boldsymbol{z}_2(t))$ has an ergodic nature which means that the statistic of wave packets $\Phi(\boldsymbol{z}_1(t),\boldsymbol{z}_2(t))$ is quantum mechanical while that of wave packet centroids is classical [39, 40]. Both the caloric curve of excited ^{16}O, ^{24}Mg, ^{27}Al and ^{40}Ca [41] and the nuclear liquid-gas phase transition during the heavy-ion collisions [42] are studied by applying the properties of time evolution of basis function.

The bound and resonant states of ^{16}O+2α system may be reasonably described by their superposition:

$$\Psi = \int_0^T dt \sum_{K=-J}^{J} f_K(t) \hat{P}^{J\pi}_{MK} \Phi(t) \tag{2.12}$$

where T is the total time-propagation length, $\hat{P}^{J\pi}_{MK}$ is the parity and angular momentum projection operator, and $\Phi(t)$ is a shorthand of $\Phi(\boldsymbol{z}_1(t),\boldsymbol{z}_2(t))$. In the practical calculations, we discretize time as,

$$\Psi = \sum_i \sum_{K=-J}^{J} f_{iK} \hat{P}^{J\pi}_{MK} \Phi(t_i) \tag{2.13}$$

$\hat{P}^{J\pi}_{MK}$ is the parity and the angular momentum projection operator of the form

$$\hat{P}^{J\pi}_{MK} = \frac{2J+1}{8\pi^2} \int d\Omega D^{J*}_{MK}(\Omega) \hat{R}(\Omega) \tag{2.14}$$

The amplitude f_{iK} and eigen-energy are calculated by the Hill-Wheeler (HW) equation [43, 44],

$$\sum_{jK'} (H_{iK;jK'} - E N_{iK;jK'}) f_{jK'} = 0, \tag{2.15}$$

where,

$$H_{iK;jK'} := \langle \hat{P}^{J\pi}_{MK} \Phi(t_i) | \hat{\boldsymbol{H}} | \hat{P}^{J\pi}_{MK'} \Phi(t_j) \rangle, \tag{2.16}$$

$$N_{iK;jK'} := \langle \hat{P}^{J\pi}_{MK} \Phi(t_i) | \hat{P}^{J\pi}_{MK'} \Phi(t_j) \rangle, \tag{2.17}$$

2.3 Calculation Procedure

In this section, we summarize the practical calculation procedure adopted for the ^{16}O+2α system. The numerical calculation performs in the following steps.

I. Imaginary-time evolution

We evolve a randomly generated ^{16}O+$\alpha+\alpha$ wave function and calculate the imaginary-time evolution of the system as follows,

$$i\hbar\frac{dz_i}{d\tau} = \mu\frac{\partial H_{int}}{\partial z_i^*} \tag{2.18}$$

where, μ is an arbitrary negative number. We obtain a state excited by $E^* := E_{int}$ - E_{min} (MeV), which serves as the initial state for the real-time evolution. E_{min} denotes the lowest intrinsic energy, which is also calculated by the imaginary time evolution. In practical calculation, we tested several choices of E^* from 20 MeV to 50 MeV.

II. Real-time evolution

We calculate the real-time evolution of the system according to the equation of motion(EOM). The time evolution was calculated with a discrete time step of Δt=0.002 fm/c, and the wave function is sampled every 2000 steps (4 fm/c) up to a maximum evolution time of T = 4000 fm/c, resulting in a maximum of 1000 sampled wave functions.

To prevent α particles from escaping to infinity, a spherical wall that reflects the α particles is placed at a distance R_{max} from the origin of the coordinate. Several values of R_{max} (from 4 fm to 9 fm) were tested. If E^* is large enough, α clusters occasionally escape out to infinite distance during the time evolution. This yields basis wave functions having unphysically large radii, which are useless for the description of the bound or resonant states. To avoid this problem, we impose an additional condition on the calculation. When the condition ($\max_i \mathrm{Re}(\frac{|Z_i(t)|}{\sqrt{\nu}}) > R_{max}$) is satisfied, i.e., if any of α clusters is distant more than R_{max}, we interchange their momentum by hand as follows: $Z_i(t+\Delta t) = Re(Z_i(t)) - iIm(Z_i(t))$, where we assume that $|Z_i(t)| > R_{max}$. We impose a rebound condition as mentioned above because the particles can move the unphysical region if they are not bound within some specific area during the time-evolution with a high excited intrinsic energy.

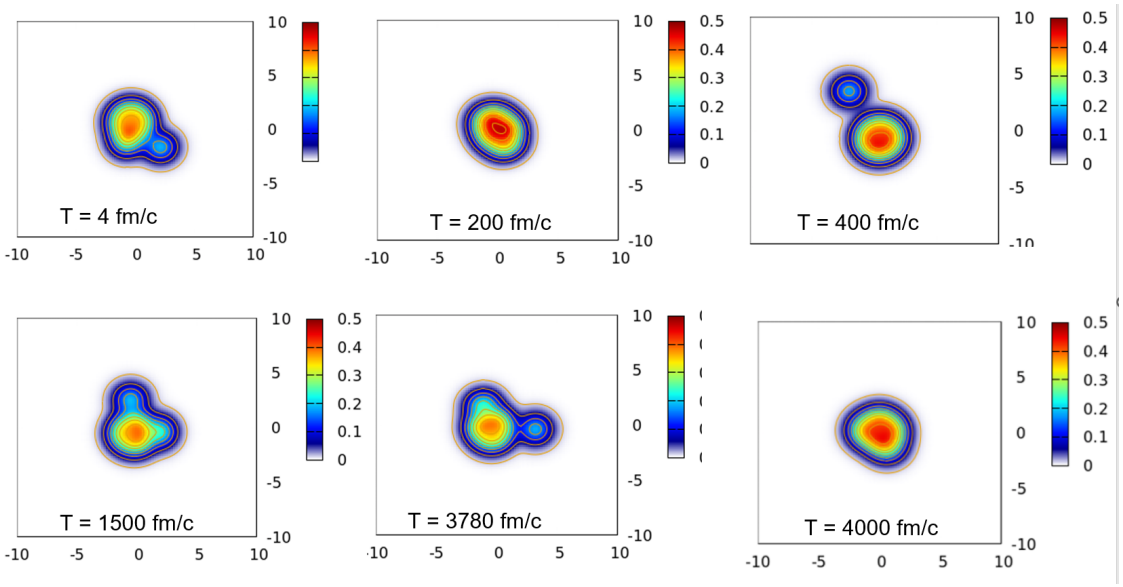

Figure 2.1: Intrinsic density snapshots of intrinsic excitation energy 30 MeV at the propagation time T=4, 200, 400, 1500, 3780 and 4000 fm/c are shown. The particles move three-dimensional space, but plane-projected here.(x and y axis are in fm)

The real-time evolution (REM) generates various configurations of basis wave functions based on the ergodic nature of the equation of motion(EOM). Therefore, if the time is propagated long enough, the results should converge and should not depend on the initial wave functions. To illustrate how the ^{16}O+α+α system evolved by the EOM, We analyze intrinsic density snapshots of wave function for intrinsic excitation energy 30 MeV for various propagation time T. According to the Fig. 2.1, the α clusters are distributed in various ways such that they are close to each other at some time and far distance another time. Actually, the system repeats a spatial expansion and contraction as time evolves, which can be confirmed from the radius of the system as a function of time. Therefore, the generated basis wave functions mainly cover different configuration of ^{16}O+α+α states according to time evolution.

III. Selection of basis functions

To avoid redundancy in the basis set, sampled wave functions with an overlap greater than 0.95 are removed. Namely, for any combination of i and j, the following condition must be satisfied,

$$\frac{\left|\langle P^{0^+}\Phi(t_i)|P^{0^+}\Phi(t_j)\rangle\right|^2}{\langle P^{0^+}\Phi(t_i)|P^{0^+}\Phi(t_i)\rangle\langle P^{0^+}\Phi(t_j)|P^{0^+}\Phi(t_j)\rangle} < 0.95 \tag{2.19}$$

where, P^{0^+} denotes the projection operator to $J^\pi = 0^+$ state. The number of remaining basis functions typically ranges from 300 to 400, depending on the calculation conditions.

IV. Solution of Hill-Wheeler equation

The selected basis wave functions are projected to the $J^{\pi} = 0^{+}$ state. The eigen energies and eigen states are obtained by solving the Hill-Wheeler equation. The calculations are prepared with different values of both the rebound radius R and the initial excitation energy E* to check the convergence of the results.

2.4 Analytic Continuation in the Coupling Constant

The method of analytic continuation in the coupling constant (ACCC) [45] includes a simple calculation method which makes it possible to calculate the characteristics of the resonance states (the resonance energies, widths, wave functions, etc.), proceeding only from the bound-state calculations.

The resonance may be treated as such an eigen state of the Hamiltonian of a system which arises from a purely bound state when the intensity of the attractive part of the interaction decreases. In the language of analytical properties, this means that a resonance S-matrix pole on the nonphysical sheet is defined as the analytic continuation of a bound-state pole on the physical sheet in the coupling constant of the attractive part of the total Hamiltonian. In the case of potential scattering, such a definition of the resonance is mathematically equivalent to the conventional definition through poles. In the particular case of the three-body problem, it may also be shown that such a definition is equivalent to the conventional definition through poles for the three-particle S-matrix which emerges from the solution of the Faddeev equations. In general case this equivalence is probable but it has not been proved rigorously yet. A characteristic feature of the present approach is that the above-mentioned obvious physical idea is realized in the theory of resonance states and the processes involving the resonance states. This theory makes it possible to describe in a unique way a broad class of phenomena in quantum-mechanical systems by studying their evolution in the coupling constant [45].

In the ACCC method, the Hamiltonian of the system is consider $H(\mu)= H_1+\mu H_2$, where H_2 is attractive part of the interaction. It introduces an attractive auxiliary potential with a parameter of μ to artificially bind the resonance states. As an auxiliary potential, we vary the strength of the exchange term of the Volkov potential in Eq. (2.2) as,

$$M = 0.63 - \mu, W = 1 - M = 0.37 + \mu, \tag{2.20}$$

where, μ is a positive number. Note that this does not change the binding energy of the α particle but makes the $\alpha - \alpha$ and ^{16}O$-\alpha$ interactions more attractive. Consequently, a larger value of μ gives deeper binding energies of ^{16}O, ^{16}O$+\alpha$ and ^{16}O$+2\alpha$ systems.

Let us denote the energy of the ground state of the ^{16}O$+\alpha$ system obtained with a certain value of μ as $E_{O+\alpha}(\mu)$, and the energy of an excited state of the ^{16}O$+2\alpha$ system as $E_{O+2\alpha}(\mu)$. Hence, $E(\mu) := E_{O+2\alpha}(\mu)$-$E_{O+\alpha}(\mu)$ is the α decay Q-value.

And, we consider an excited state of the ^{16}O+2α system which is unbound at the physical point (μ=0), i.e., E(0) > 0. As the value of μ increases, this state becomes bound. That is, E(μ_0) = 0 for a certain value of μ_0, and E(μ) < 0 holds for $\mu > \mu_0$. Note that in the region E(μ) < 0 ($\mu > \mu_0$), the eigen state can be accurately calculated within a finite spatial domain. However, this is not the case for $\mu < \mu_0$, where the exact solution is not square integrable. Therefore, the ACCC method analytically continues the solution from the region $\mu > \mu_0$ into the region $\mu < \mu_0$, allowing us to determine the resonance energy and width at the physical point.

Practically, following the procedure in [46, 47], we introduce a variable $x = \sqrt{\mu - \mu_0}$. Then, $\varepsilon(x) := E(\mu)$ is written as,

$$\varepsilon(x) = \frac{\hbar^2}{2m} k^2(x) \tag{2.21}$$

$$k(x) = i \frac{c_1 x + ... + c_M x^M}{1 + d_1 x + ... + d_N x^N}, \tag{2.22}$$

where m is the reduced mass and the wave number $k(x)$ is expressed by the rank [M/N] Pade approximation. The coefficients $c_1, ..., c_M, d_1, ..., d_N$ are determined by the fitting in the region $\mu > \mu_0$. Finally, Eq. (2.21) and Eq. (2.22) are extrapolated to the physical point, $\mu = 0$. That is, the resonance energy E_R and width Γ_R are evaluated at the physical point $x_0 = i\sqrt{\mu_0}$,

$$\varepsilon(x_0) = \frac{\hbar^2 k^2(x_0)}{2\mu} = E_R - i\frac{\Gamma_R}{2}, \tag{2.23}$$

where, E_R and Γ_R denote the resonance energy and width, respectively. In the practical calculation, we found that M = N = 6 is large enough to obtain the stable results.

Chapter 3

Results and Discussions

In this chapter, we discuss the results of gas-like bosonic states formed around the ^{16}O+$\alpha + \alpha$ threshold energy.

3.1 Convergence of the eigen states by Stabilization Method

In this section, we present how the calculation results converge with a long-time evolution. We also show how the results depend on the numerical conditions, such as the rebound distance R and the intrinsic energy E*.

Before the calculation of eigen energies by Real Time Evolution(REM), we compare the ground state energy of α particle and ^{16}O with the result of Ichikawa et al. [33]. As a first step, we randomly generates the initial wavefunctions for α particle and apply it to find the ground state energy by using variational method with the present interaction and model space. The calculated binding energy of α particle is -27.6059 MeV and the numerous output eigen energies values are unchanged since the energy of α particle is position independent.

Next, the ground state energy of ^{16}O, which is in the form of tetrahedron configuration of four α particles with the relative distance 0.5 fm, has been calculated . The resulted ground state energy of ^{16}O is -118.2 MeV compared with the experimental value of -127.6 MeV. The Ichikawa et al. reported that -118.8 MeV is the energy of ^{16}O in tetrahedron configuration of four α's with the relative distance 0.5 fm. Therefore, there is slightly different result between our calculation and Ichikawa et al.

We perform basis wavefunction of ^{16}O+2α for various configuration and calculate the minimum energy of intrinsic state of ^{16}O+2α. The minimum energy of the intrinsic state of ^{16}O+2α is approximately -173.473 MeV and memorize as a ground state energy of the

^{16}O plus two α system. However, the result of Ichikawa et al. [33] is mentioned as 16.63 MeV from the ground state of ^{24}Mg(-173.11 MeV). Therefore, The minimum energy of intrinsic state of ^{16}O+2α is much shallower than Ichikawa et al. report even though we have performed the parity-angular momentum projection.

Now, we explain Real-time evolution calculation is performed for 6α cluster system(^{24}Mg) with various ^{16}O+$\alpha+\alpha$ configuration and calculate the imaginary-time evolution of the system as shown in Eq.(2.18). This imaginary-time evolution is continued until the intrinsic excitation energy of 35 MeV and the rebound distance R = 7 fm. Figure (3.1) mentions how the eigen energies converge as a function of the evolution time T, under the condition of E* = 35 MeV and rebound distance R = 7 fm. The 0^+_1 and 0^+_2 states are the bound states lower than the α-decay threshold. After long-time evolution, their energies are slightly lower than those calculated by Ichikawa et al [33], which indicates an improvement by Real-time Evolution method compared to the randomly generation of the basis wave function.

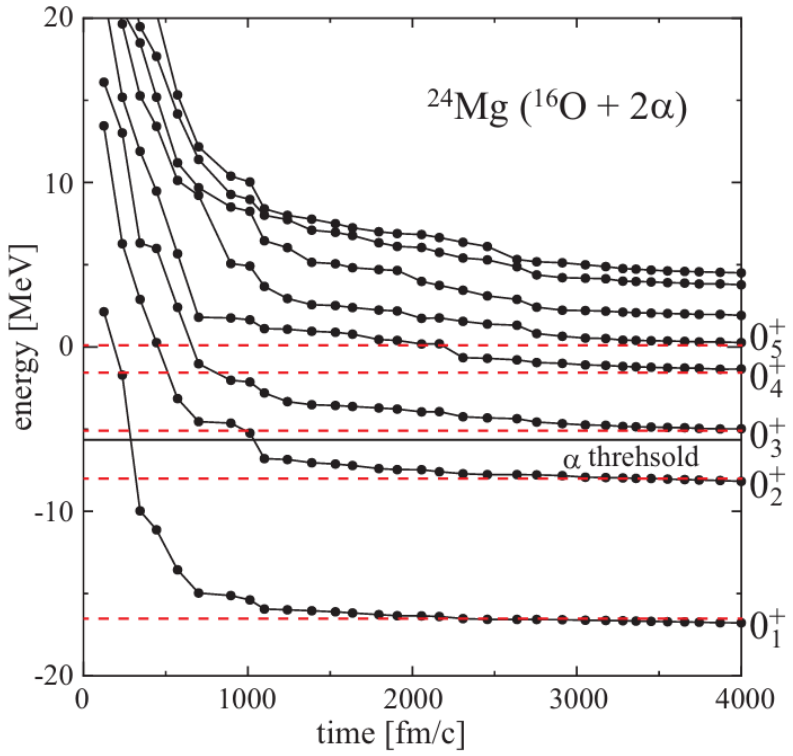

Figure 3.1: The energies of the 0^+ states obtained with the time evolution up to T [fm/c]. The dotted line shows the calculated α decay threshold. The red dashed lines show the energies of the bound states and resonance candidates suggested in Ref. [33]

For unbound states above the threshold (0_3^+ and higher states), the energy slowly decreases over time due to coupling with the continuum. Nevertheless, the obtained result plausibly agrees with the candidates of ^{16}O+2α resonances proposed in Ref [33]. Compared to the random basis generation, the coupling with the continuum is significantly weaker in REM calculation. It means that the Real-time Evolution method reduces the coupling effect with continuum in the resulted eigen energies.

For highly excited states above the ^{16}O+2α threshold (0_5^+ and above excited states), however, the coupling with non-resonant states is strong, and we could not clearly distinguish between resonant and non-resonant states.

In result of Ichikawa et al., numerous eigen energies below the ^{16}O+2α threshold are obtained because the basis wave function is generated randomly since many continuum states are mixing into the results. Most of which were discarded as non-resonant solutions due to their instability. In the results of Real-time Evolution method calculation, the particles are confined within a finite radius and the basis wave function is generated by physical equation of motion. The results of Real-time Evolution method are free from instability, allowing for the unique identification of resonance states. Therefore, we can expect that there is less mixing with continuum states.

To analyze the convergence of the eigen energies, Hazi and Taylor proposed that the idea of stabilization method [48] at 1970. The Stabilization method can be applied not only proceeding from the similarity between a resonance state (especially narrow resonance) and a bound state but also in the classical stabilization procedure. The method idea works by placing a system into a box with infinite walls will not disturb the resonance spectrum significantly.

In our calculation, the Hamiltonian of the system is diagonalized in a quadratically integrable basis wave function. We perform the first boundary conditions such as the confinement radii between 4 fm to 9 fm imposed on the basis wavefunction. And the second boundary conditions is changing the intrinsic excitation energy when we performed the Real-time evolution calculation. According to the stabilization idea, the energy of the resonance should not depend so much on confinement radii and intrinsic excitation energies, conversely, the energy of non-resonant continuum depends on the calculation boundary conditions. We analyzed stability of the energies of 0^+ states by using "Stabilization method".

As a first step, we examine the convergence by varying the rebound radius R. Figure (3.2) shows how the eigen energies depend on the reflection radius R with fixed E* = 35 MeV and T = 4000 fm/c. It was found that the energies of the first to fifth 0^+ states do not change significantly depending on the rebound radius. These suggest that they are resonant states since the 0_1^+ and 0_2^+ states are bound states. While we analyze at the 0_1^+ and 0_2^+ states in detail, they are more deeply bound when the rebound radius is R = 6 or 7 fm. At smaller rebound radii, R = 4 or 5 fm, the spatial size seems to be too small, whereas at larger radii of R = 8 or 9 fm, a sufficient number of states could not be generated within the finite time evolution (4000 fm/c).

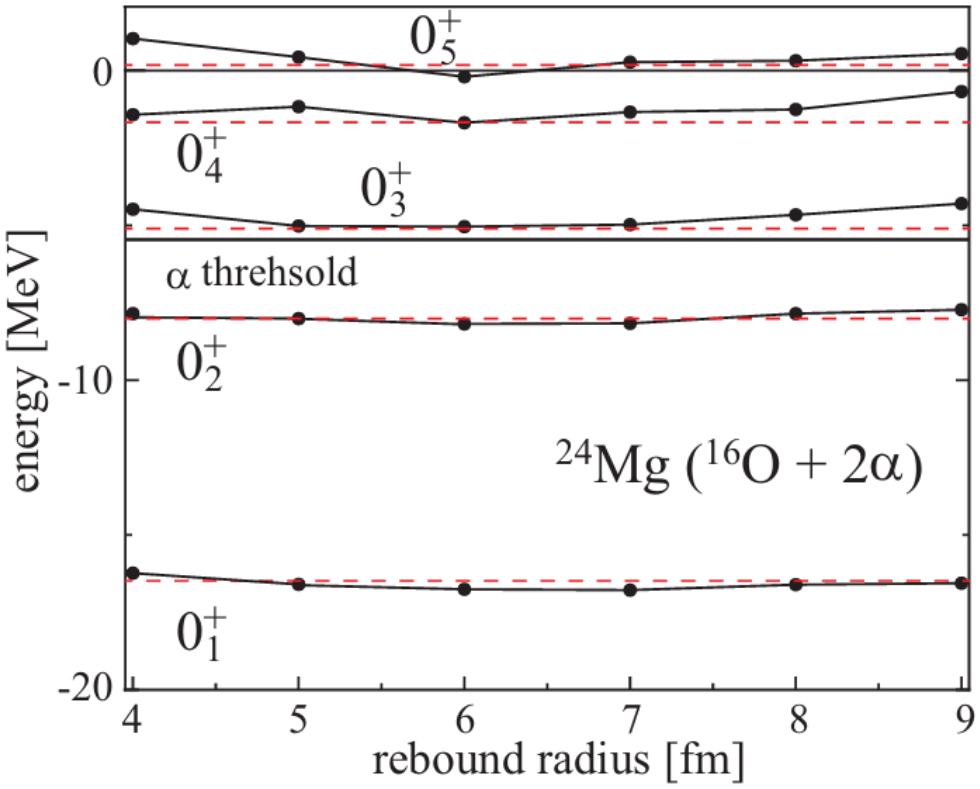

Figure 3.2: The energies of the five lowest 0^+ states obtained after the time evolution up to T = 4000 [fm/c] with the same energy E* = 35 MeV, but different rebound radii R = 4,...,9 fm. The dotted line shows the calculated α decay threshold. The red dashed lines show the energies of the bound states and resonance candidates suggested in Ref. [33]

And, as a second step, we continued the analysis how the eigen energies depend on the intrinsic excitation energy E* applied in solving the Equation of Motion(EOM). First, we notice that approximately consistent and reliable results are obtained in the region of E* from 30 to 40 MeV. At intrinsic energy E* = 25 MeV, the energy of the excited state is overestimated. Since the intrinsic energy is too small, the α particle could not cross the Coulomb barrier and moved only within a space smaller than R = 7 fm.

On the other hand, for E* $\geq$ 45 MeV, the energies of the low-lying excited states are overestimated, which is likely because the generated ensemble did not span the model space large enough to describe the low-lying states due to a higher value of intrinsic energy E*. Thus, the results obtained at rebound radius R = 7 fm and 35 MeV intrinsic excitation energy are seem reasonable, and the discussion in the next section is based on these data.

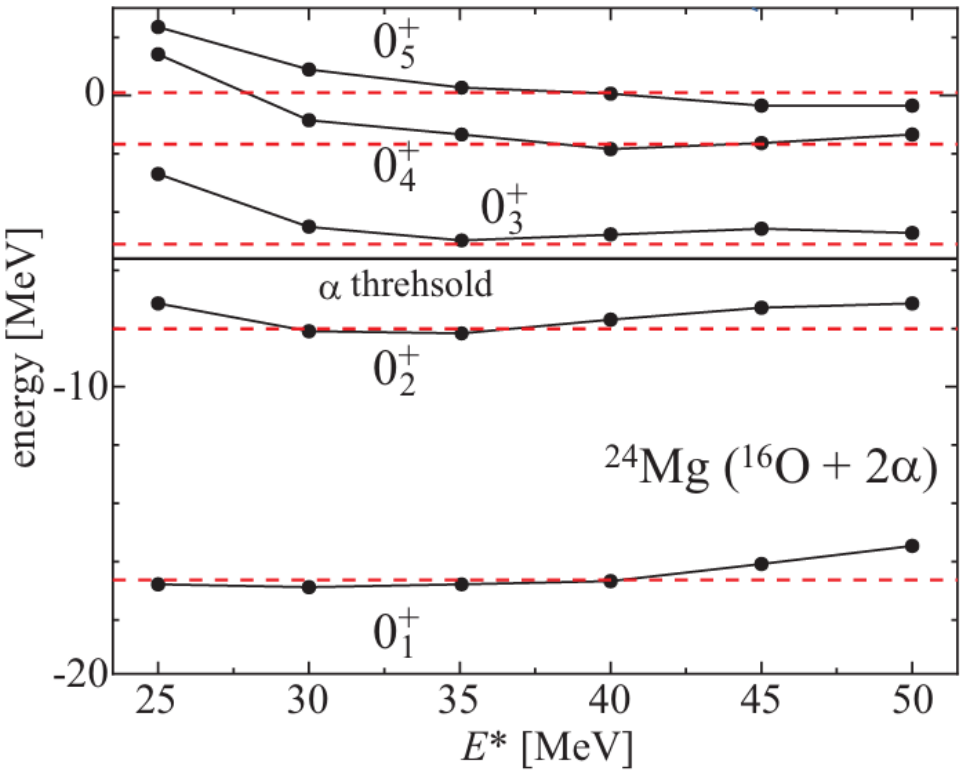

Figure 3.3: The energies of the five lowest 0^+ states obtained after the time evolution up to T = 4000 [fm/c] with the same rebound radius R = 7 fm, but different intrinsic energies E* = 25, ..., 50 MeV were applied for solving Equation of Motion(EOM). The red dashed lines show the energies of the bound states and resonance candidates suggested in Ref. [33]

3.2 Properties of the resonance candidates

In this section, we examine the properties of the resonance candidates obtained in the previous section. Table (3.1) summarizes their properties: the energies, widths, isoscalar monopole transition strength from the ground state and radii.

Table 3.1: The properties of the first five 0^+ states: energy (MeV), width (MeV), isoscalar monopole transition strength from the ground state (fm^4), and radius (fm). The data for the 0_3^+ and 0_4^+ states are evaluated by ACCC, while ACCC was not applicable for the 0_5^+ state.

state	E	Γ	B(ISO)	$\sqrt{\langle r^2 \rangle}$	$\sqrt{\langle r^2 \rangle_{val}}$
0_1^+	-16.78	-	-	2.67	3.47
0_2^+	-8.16	-	28.4	2.70	3.53
0_3^+	-4.95	≤ 0.01	145.0	2.97	4.13
0_4^+	-1.26	0.17	160.7	2.94	4.08
0_5^+	0.37	-	4.28	3.03	4.28

For the bound states (0_1^+ and 0_2^+ states), as mentioned above, the present calculations yield slightly deeper binding energies compared to Ref. [33] (-16.63 MeV and -8.01 MeV, respectively). In contrast, the energies of the 0_3^+ and 0_4^+ states are slightly higher. This is due to the decoupling of the continuum states by the ACCC method. Their widths, especially that of the 0_3^+ states, are small, suggesting that they are experimentally observable. However, we must consider the proton decay channel, whose threshold is located at -5.09 MeV. Although the proton decay is outside our model space, its impact on the 0_3^+ state seems to be minor, since the decay Q-value is quite small. In contrast, its influence on the 0_4^+ state may be non-negligible and evaluating it with a microscopic model is a future task. For the 0_5^+ state, we were unable to obtain the stable solution of ACCC because its energy is too high above the α threshold to be extrapolated from the bound state region.

Next, we examine the isoscalar monopole transition strength from the ground state to resonance candidates, B(IS0), which characterizes spatially extended cluster states [49]. As pointed out by Ichikawa et al., [33], the transition strengths of the 0_3^+ state and 0_4^+ state are remarkable. Quantitatively, our calculated results are very close to their results (143.80 fm^4 and 152.98 fm^4, respectively), which further supports the argument that they are candidates for the ^{16}O+2α condensate.

Finally, we discuss about the root mean square radii of each states. Although these radius cannot be strictly defined for resonance states, that calculated within the bound-state approximation provides a measure of the spatial extent of the interaction clusters. While the radii of the bound states are around 2.7 fm, the root mean square radii of the 0_3^+ and 0_4^+ states are approximately 3.0 fm, showing some increase. This is also in good agreement with the values obtained by Ichikawa et al [33]. The root mean square radii of the 0_3^+ and 0_4^+ states seem small compared to that of the Hoyle state of ^{12}C (3.7 fm). However, this comparison may not be straightforward since the contribution from the inert core, ^{16}O, should be subtracted.

Therefore, we define the distribution radius of the valence 2α particles around the core as follows:

$$\langle r^2 \rangle_{val} := \frac{1}{8} \sum_{i \in valence} r_i^2 = 3\langle r^2 \rangle_{O+2\alpha} - 2\langle r^2 \rangle_O \tag{3.1}$$

where, $\langle r^2 \rangle_{O+2\alpha}$ and $\langle r^2 \rangle_O$ denote the root mean square radii of the ^{16}O+2α system and the ^{16}O core, respectively. Based on this, the distribution radii of the 2α particles around the core are calculated in Table (3.1). It can be seen that the distribution radii of the valence α particles in the 0_3^+ and 0_4^+ states are even larger than that of the Hoyle State. Furthermore, the distribution radii of the valence α particles in the 0_3^+ and 0_4^+ states (4 fm) roughly coincide with the expected radius of the Coulomb barrier of the ^{16}O+α, suggesting the 0_3^+ and 0_4^+ states have α particles trapped between the surface of the core nucleus and the Coulomb barrier.

Chapter 4

Conclusion

The search for core nucleus+nα condensates where α particles condense around an inert core nucleus, is an interesting problem, offering a novel type of α clustering. Previous theoretical works suffered from significant mixing with physically unimportant configurations, making the clear identification of real resonances difficult.

To address these limitations and further investigation about the predictions of the ^{16}O+2α condensate by Ichikawa et al., we employed Real Time Evolution method to generate physically important basis wave functions with less contamination from the continuum. Furthermore, we applied the ACCC to estimate the α-decay widths of the resonance candidates.

The numerical results of Real Time Evolution method show reasonable agreement with those of Ichikawa et al. and firmly establish the candidates for the ^{16}O+2α condensed state. The REM successfully generated cleaner ensembles, aiding in the identification of resonance states. Especially, the 0_3^+ and 0_4^+ states were identified as strong candidates. These states exhibited remarkably enhanced isoscalar monopole transitions from the ground state to various excited states , quantitatively, close to previous findings, strongly supporting their nature as spatially extended ^{16}O+2α condensate. The valence 2α distribution radii for these states (around 4 fm) were comparable with the expected radius of the Coulomb barrier around ^{16}O, suggesting the α particles might be trapped by the barrier. The calculated α-decay widths of the 0_3^+ and 0_4^+ states were small, suggesting that they should be experimentally observable. The Real-time evolution method (REM) proved effective in identifying these states.

Bibliography

[1] D. Halliday, Introductory Nuclear Physics, pg. 261 (1955).

[2] M. Freer, H.O.U. Fynbo / Progress in Particle and Nuclear Physics **78** (2014) 1–23.

[3] M. G. Mayer, Phys. Rev. **75** (1949), 1969.

[4] O.Haxel, J. H. D. Jensen and H. S. Suess, Z. Phys. 128 (1950), 295.

[5] Y. Abe, H. Horiuchi, K. Ikeda, M. Kamimura, K. Kato, S. Okabe, S. Saito and Y. Suzuki, Soryushiron Kenkyu (Kyoto) **58** (1978), B1.

[6] J. Hiura, Y. Abe, S. Saito and O. Endo, Prog. Theor. Phys. **42** (1969), 555.

[7] K. Ikeda, et. al., Prog. Theor. Phys. Suppl. **464** (1968).

[8] K. Ikeda, T. Marumori, R. Tamagaki and H. Tanaka, Prog. Theor. Phys. Suppl. No. 52 (1972). 1.

[9] M. H. Anderson et al., Science 269, **198** (1995).

[10] F. Hoyle, Astrophys. J. Suppl. Ser. **1** (1954) 121.

[11] E. Öpik, Proc. R. Ir. Acad. A **54** (1951) 49.

[12] E.E. Salpeter, Astrophys. J. **115** (1952) 326.

[13] E. Uegaki et al., Prog. Theor. Phys. **59** (1978) 1031.

[14] M. Kamimura, Nucl. Phys. A **351** (1981) 456.

[15] R. Bijker and F. Iachello, Phys. Rev. C **61** 067305 (2000).

[16] R. Bijker and F. Iachello, Prog. Part. Nucl. Phys. **110** 103735 (2020).

[17] P Schuck, et al., J. Phys.: Conf. Ser. **863** 012005 (2017).

[18] T. Yamada and P. Schuck, Eur. Phys. J. A **26** (2005) 185.

[19] Y. Funaki et al., Phys. Rev. C **80** 064326 (2009).

[20] A. Tohsaki, H. Horiuchi, P. Schuck, and G. R¨opke, Phys. Rev. Lett. **87** 192501 (2001).

[21] Y. Funaki, A. Tohsaki, H. Horiuchi, P. Schuck, and G. R¨opke, Phys. Rev. C **67** 051306 (2003).

[22] S. Shen, S. Elhatisari, T. A. L¨ahde, D. Lee, B.-N. Lu, and U.-G. Meißner, Nature Communications **14** 2777 (2023).

[23] Y. Funaki, T. Yamada, H. Horiuchi, G. Ropke, P. Schuck and A. Tohsaki, Phys. Rev. Lett. **101** 082502 (2008).

[24] T. Yamada, Y. Funaki, H. Horiuchi, G. R¨opke, P. Schuck, and A. Tohsaki arXiv:1103.3940 (2011)

[25] P. Schuck, Y. Funaki, H. Horiuchi, G. R¨opke, A. Tohsaki, and T. Yamada, Phys. Scripta **91** 123001 (2016).

[26] S. Adachi et al., arXiv:2008.01632,(2021).

[27] B. Zhou et al., Nat. Commun. **14** 8206 (2023).

[28] Y. Fujikawa et al., Phys. Lett. B **848** 138384 (2024).

[29] T. Yamada and P. Schuck, Phys. Rev. C **69** 024309 (2004).

[30] Tz. Kokalova et al., Eur. Phys. J. A **23** 19 (2005).

[31] N. Itagaki, M. Kimura, C. Kurokawa, M. Ito and W. von Oertzen, Phys. Rev. C **75** 037303 (2007).

[32] N. Itagaki, T. Kokalova, and W. von Oertzen, Three-alpha state around ca40, Physical Review C **82** 014312 (2010).

[33] T. ICHIKAWA et al., Phys. Rev. C **83** 061301(R) (2011).

[34] A. Volkov, Nucl. Phys. **74** 33 (1965).

[35] Y. Fujiwara, H. Horiuchi, K. Ikeda, M. Kamimura, K. Kato, Y. Suzuki, and E. Uegaki, Prog. Theor. Phys. Suppl. 68, 29 (1980).

[36] D. M. Brink, in Proceedings of the International School of Physics Enrico Fermi, Course 36, Varenna, edited by C. Bloch(Academic Press, New York, 1966).

[37] R. Imai, T. Tada, and M. Kimura, Phys. Rev. C **99**, 064327 (2019).

[38] J. Schnack and H. Feldmeier, Nucl. Phys. A 601, 181 (1996).

[39] A. Ono and H. Horiuchi, Phys. Rev. C **53** 2341 (1996).

[40] A. Ono and H. Horiuchi, Phys. Rev. C 53, 845 (1996).

[41] J. Schnack and H. Feldmeier, Phys. Lett. B 409, 6 (1997).

[42] Y. Kanada-En'yo, M. Kimura, and A. Ono, Prog. Theor. Exp. Phys. 2012, 1A202 (2012).

[43] D. L. Hill and J. A. Wheeler, Phys. Rev. **89 1102 (1953).**

[44] J. J. Griffin and J. A. Wheeler, Phys. Rev. 108 311 (1975).

[45] V. I. Kukulin and V. M. Krasnopol'sky, Journal of Physics A: Mathematical and General 10, L33 (1977).

[46] N. Tanaka, Y. Suzuki, and K. Varga, Phys. Rev. C 56 562 (1997).

[47] R. Takatsu, Y. Suzuki, W. Horiuchi, and M. Kimura, Phys. Rev. C 107, 024314 (2023).

[48] A. U. Hazi, H. S. Taylor, Phys. Rev. A1 (1970) 1 109.

[49] T. Yamada, Y. Funaki, H. Horiuchi, K. Ikeda, and A. Tohsaki, Prog. Theo. Phys. 120, 1139 (2008).